Quarterly Progress Report 2

Radar Studies of the Moon

15 May 1966

Issued 2 June 1966

Prepared for the U.S. National Aeronautics and Space Administration
under Contract NSR 22-009-106 by

Lincoln Laboratory

MASSACHUSETTS INSTITUTE OF TECHNOLOGY

Lexington, Massachusetts

FOREWORD

This is the second Quarterly Progress Report required under Contract NSR 22-009-106 between the National Aeronautics and Space Administration and Lincoln Laboratory, M.I.T. In addition to covering the first four months' work under the contract, the first progress report reviewed in considerable detail the work performed and the methods used to study the lunar surface by radar up to the time of the start of the contract period. In the present and subsequent progress reports frequent reference will be made to this review material and the plans described in the first report [referred to as QPR (1966:1)].

Section I of the present report covers the more important aspects of the research completed under the contract during the period 1 February through 30 April 1966. It also briefly explains certain additional experiments which were carried out during the period; some of the results will be reported in detail in the next quarterly report. This section contains some theoretical material pertaining to the effect of shadowing on the backscattering from a rough surface.

Section II contains some information on the plans and the present status of the 8-mm radar work. A survey is also presented of the considerable progress in the development of both the hardware and software necessary for mapping at 3.8 cm.

Section III contains a discussion of possible future experiments, not previously planned, whereby the depth of the surface layer may be measured.

CONTENTS

I. RESEARCH RESULTS

A. SCATTERING PROPERTIES AT 23 cm

1. Introduction

Short pulse studies of the lunar surface have been made at a number of wavelengths. These measurements are, in our view, usually to be preferred to other types such as power spectrum measurements, discussed by Evans and Pettengill (1963a), for the following reasons: (a) better resolution can be obtained by examining the distribution of echo power with respect to delay rather than frequency owing to the small angular rotation rate of the moon (an exception is the area near the subradar point), (b) there is a direct correspondence between the echo power at a given range delay t and the angle of incidence and reflection φ of the radio waves, and (c) for practical reasons it is often possible to explore the echo power over a larger dynamic range when separating the echoes with respect to range, than when resolving them in frequency.

The scattering properties of the lunar surface were previously explored over almost the full range of angles $0 < \varphi < 90°$ at 3.6- and 68-cm and 6-m wavelengths. Table I lists the observations made thus far, together with those reported here. The pulse lengths used in these measurements and also the intervals at which the echo power was sampled (Table I) differed considerably. It can be seen that prior to the present measurements the behavior in the region 10 to 90° had been observed only at wavelengths of 3.6, 68 and 600 cm. In addition, the pulse lengths employed prevented a useful examination of the region $\varphi < 10°$ at all but two wavelengths, namely 10 and 68 cm. During the observations at 23-cm wavelength reported here, experiments were conducted to match the resolution achieved at 3.6- and 68-cm wavelength, and the scattering behavior has been explored over all φ for both the expected and depolarized components of the echo.

2. Observational Procedure

The observations reported herein at 23-cm wavelength were made using the Lincoln Laboratory, Millstone Hill Radar (42.6°N, 71.5°W). The system parameters employed are listed in Table II. The antenna was directed to point continuously at the center of the moon's disk by means of a Univac 490 digital computer or by automatic readings of a prepared punched paper tape which gave pointing instructions at 10-sec intervals. Checks could be made by means of a television camera aligned along the axis of the beam to confirm that the pointing was accurate. The receiver was tuned to within 0.1 cps of expected frequency of the echo by means of a special linearly varying frequency generator, the slope of the linear frequency variation being reset at 5-minute intervals. In addition to guiding the receiver tuning in frequency to match the expected Doppler shift, the variation of the position of the echo on the time-base due to the continuously changing range was compensated to within a small fraction of the pulse length. In this way samples of the echo intensity could be taken at fixed delays with respect to the echo position, and these could be averaged to obtain the mean echo power at that delay. The manner in which these range and frequency compensations are provided has been described elsewhere (Evans, et al., 1965).

TABLE I

ANGULAR POWER SPECTRUM STUDIES OF THE MOON

Wavelength (cm)	Observer	Pulse Length	Sample Interval	Range of ϕ studied (degrees)	Comments
0.86	Lynn, et al. (1963)	2 sec	once per pulse	8 – 60	Angular resolution achieved using 0.07° pencil beam
3.6	Evans & Pettengill (1963b)	30 μsec	20 μsec	5 – 80	
10	Hughes (1961)	5 μsec	20 μsec	2.5 – 14	Sensitivity limitations prevented higher values of ϕ from being examined.
23	This report	10 μsec	10 μsec	2.5 – 90	
68	Evans & Pettengill (1963b)	12 μsec	10 μsec	2.5 – 90	
600	Klemperer (1963)	100 μsec	?	7.5 – 90	
1130	Davis and Rohlfs (1964)	250 μsec	250 μsec	12 – 48	Echoes read from film.

TABLE II

MILLSTONE L-BAND RADAR PARAMETERS

Frequency	1295.0 Mcps
Antenna	84-ft parabola with Cassegrain feed arrangement
Antenna Gain	47.3 db
Polarization	right circular transmitted right and left circular separately received
Beamwidth	0.6° between half power points
Transmitter Power	variable, 5-MW peak maximum (continuously monitored)
Pulse Length	variable, pulses 10 to 200 μsec long were employed in these observations
Receiver Bandwidth	100- or 50-kcps predetector. Postdetector filter matched to 10-μsec pulses for 10-μsec pulse transmissions, matched to 20-μsec pulses for all other transmissions.
System Noise Temperature	~150°K (continuously monitored)
Overall feed-line and other losses	2.1 db

Following the last frequency conversion in the multiple superheterodyne receiver the signal is applied to a pair of phase detectors, which are driven at the same reference frequency but shifted in phase by 90°. The outputs of these detectors are thus the sine and cosine components of the signal. These components are separately filtered by low-pass filters and sampled by identical digital voltmeters. The voltmeters are commanded to take samples at equal intervals of delay. A choice of several sampling frequencies is available. Most of the measurements were conducted with sampling frequencies of 50 or 100 kcps.

The time required for the voltmeter to make a determination is 0.25 μsec. Each voltmeter determines the sign of the signal and assigns it one of 32 possible levels. The total dynamic range of the receiver system is therefore limited by these voltmeters to 30 db. The echo intensity could be explored over a wider range than this, however, by raising the transmitter power and repeating the measurements at different signal-to-noise levels. The samples obtained in this fashion were recorded digitally on magnetic tape for later computer processing.

In the simplest form of processing the pair of samples corresponding to a given range delay are squared and added to yield the echo power at that delay. This sum is then added to all other sums for that delay to yield an average for the echo power at that delay.

The 23-cm system contains two complete channels like the above, making it possible to receive and record the two orthogonally polarized components of the signals simultaneously. In this way the polarization of the reflected signals could be explored.

3. Power vs Range, Polarized Component

In this measurement a circularly polarized wave of one sense was transmitted and the opposite (i.e., the expected sense) was received. In order to explore the echo power P(t) over the complete radar depth of the moon (11.6 msec) observations conducted with a variety of pulse lengths were carried out.

The echo power was established for the region of delays 0 to 700 μsec using a pulse 10 μsec long and a sampling interval of 10 μsec. Observations were also made in which 30-μsec pulses with a 20-μsec sample interval were used. For both sets of observations the transmitter power was lowered to ensure that the echo power did not exceed the maximum sampling level of the digital voltmeters. These measurements were then repeated at a somewhat higher power to establish the dependence in the region 0 to 2.4 msec, yielding finally the results plotted in Fig. 1.

Observations made with 30-, 100- and 200-μsec pulses and corresponding sample intervals of 20, 100 and 200 μsec were then used to establish the curve in the region 2.4 to 11.6 msec. These observations are plotted in Fig. 2.

Since the antenna beam of the Millstone radar has a half power beam-width comparable to the angular extent of the moon it was necessary to correct the observations for the non-uniform

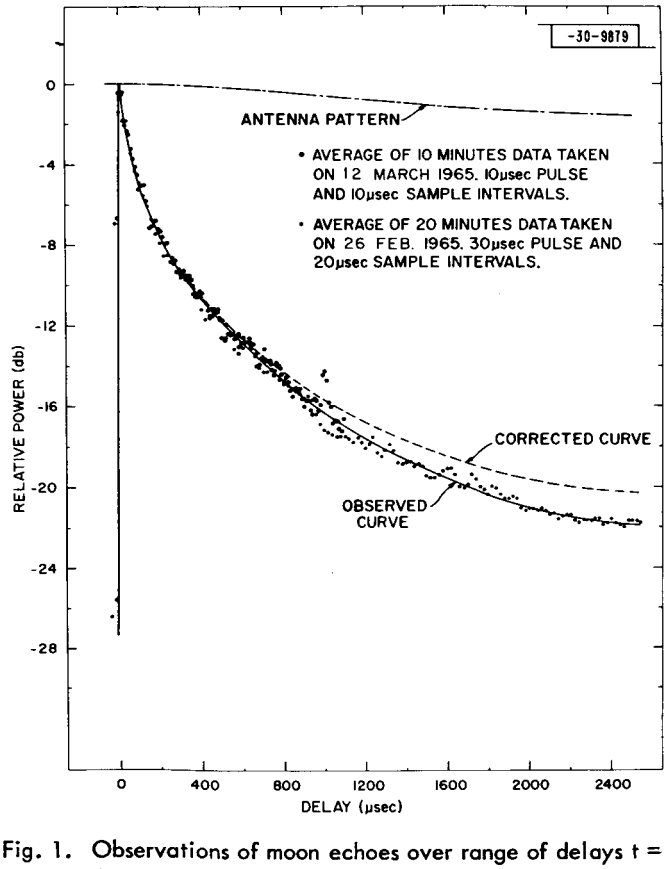

Fig. 1. Observations of moon echoes over range of delays t = 0 to t = 2.4 msec at 23-cm wavelength.

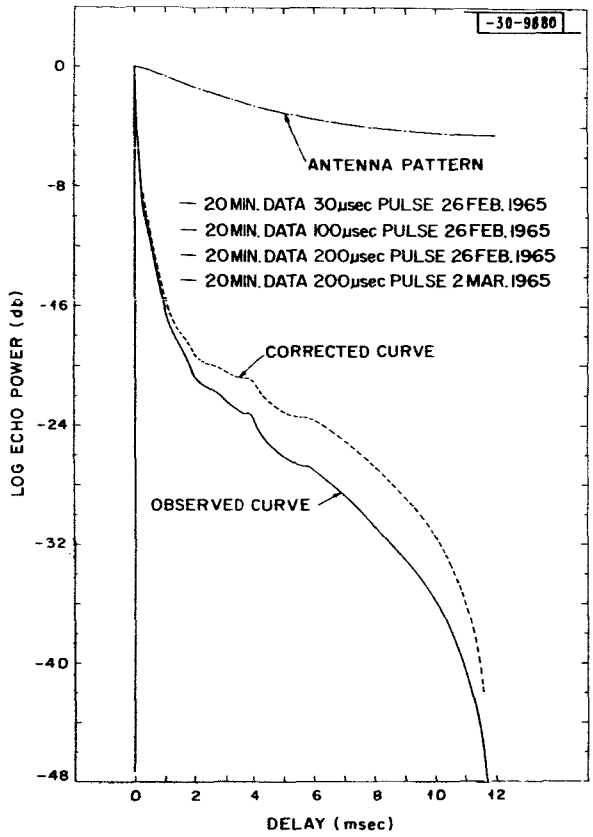

Fig. 2. Observations of moon echoes over full range of delays 0 to 11.6 msec using pulses of 30, 100, and 200 μsec. Dashed curve was obtained by correcting observations for effect of non-uniform illumination introduced by antenna beam, and has been taken to give variation of echo power of range of delays 2.4 to 11.6 msec.

illumination of the moon's surface. The antenna radiation pattern (Fig. 3) was established using radio stars and a distant beacon transmitter as sources. Both methods agreed well and Fig. 3 presents a pattern obtained by averaging plots obtained for the azimuth and elevation planes. Since the moon has a diameter of 0.5° the antenna pattern correction required is not large, amounting to only 4db at the limbs. (Note that the antenna weights the transmission and reception equally so that the effect must be included twice.)

In Figs. 1 and 2 we have shown the corrected curve of echo power vs delay P(t) obtained when the effect of the antenna has been removed. The corrected curves were next replotted as functions of the logarithm of the echo delay, t, and overlaid to obtain a single smooth curve. In this way we remove the effect of the saturation of the receiver encountered at the leading edge when attempting to observe the limbs. Figure 4 shows the results obtained.

The values plotted in Fig. 4, together with the values observed at 3.6- and 68-cm wavelengths by Evans and Pettengill (1963b), were included in Radar Studies of the Moon Quarterly Progress Report (1966:1) as Table III. Figure 5 shows the results obtained at the three wavelengths

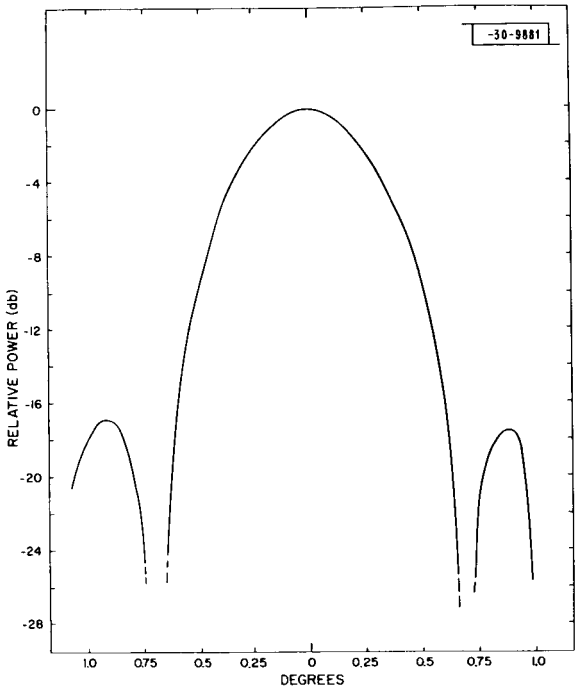

Fig. 3. Antenna pattern for Millstone Hill 1295 Mcps radar obtained by scanning radio stars and a distant beacon transmitter. Pattern shown imposes a weighting of results both on transmission and reception. Effect of this weighting is indicated in Figs. 1 and 2.

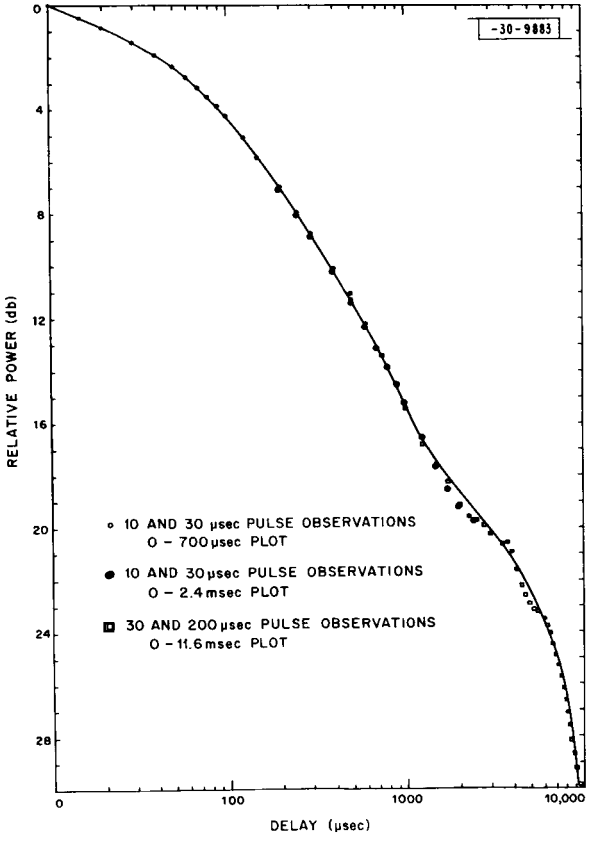

Fig. 4. Plot of combined results of all measurements at 23-cm wavelength to obtain complete dependence of echo power with delay.

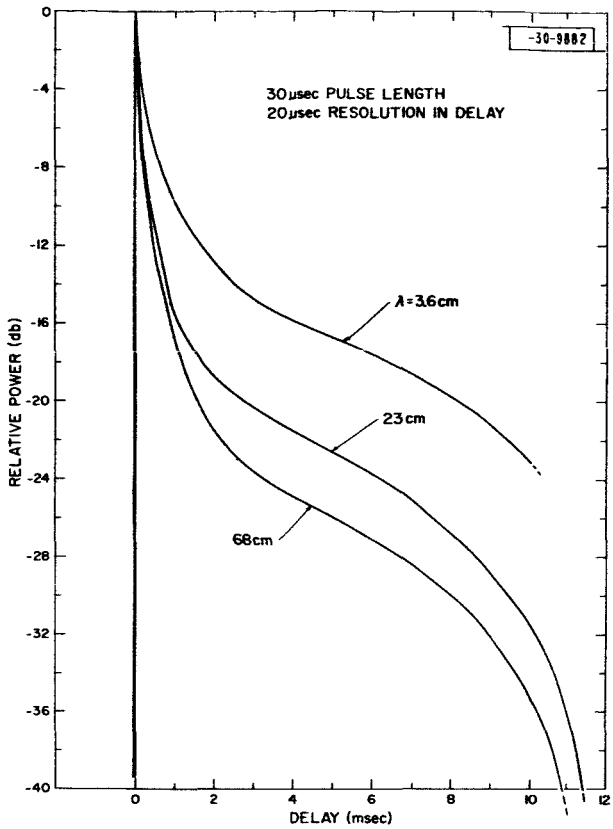

Fig. 5. Comparison of 23-cm results shown in Fig. 2 with results reported by Evans and Pettengill (1963b) at 3.6- and 68-cm wavelengths.

when pulses of 30 μsec are used to resolve the leading edge. These three curves have been normalized at the origin and are the only results at different wavelengths in which exactly the same resolution was employed.

4. Power vs Range, Depolarized Component

By receiving the same sense of circular polarization as was transmitted it is possible to determine the amount of power that has been converted into the orthogonal circularly polarized mode. Evans and Pettengill (1963b) called this component the "depolarized" component, though additional measurements using linearly polarized waves are required if the complete scattering matrix for the surface is to be established. With the Millstone system, measurements of the depolarized and polarized components could be made simultaneously, or alternately at will.

Figure 6 shows the distribution of depolarized echo power, D(t), vs delay, obtained for the depolarized component. Up to a delay of 4 msec, 160-μsec pulses, 50-kcps predetection filters and a sample interval of 160 μsec were used, while 1-msec pulses, 2-kcps predetection filters and a sample interval of 480 μsec were used for delays beyond 4 msec. The absolute level of the echo can be established by injecting into the receiver input terminals (via a directional coupler) a pulse of noise corresponding to a known increase in system temperature on each sweep of the time-base. This pulse served to determine the relationship between D(t) and the polarized

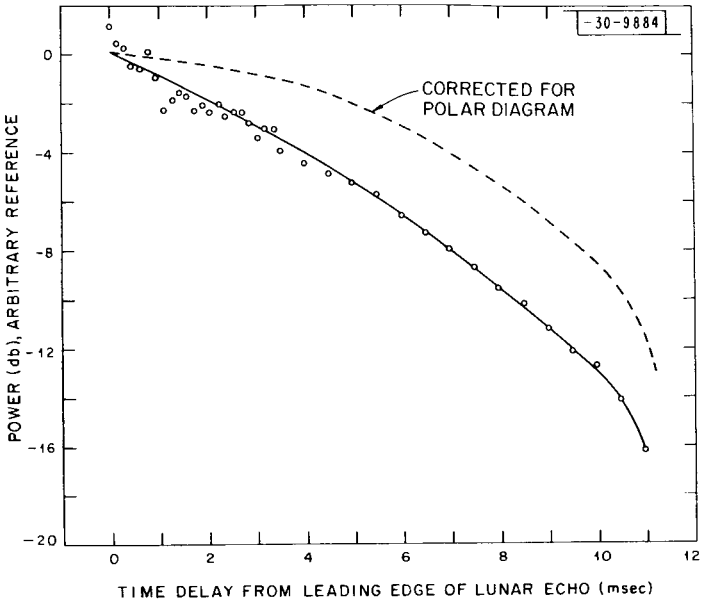

Fig. 6. Depolarized or opposite sense circularly polarized mode observed at 23 cm wavelength on 3 Feb. 1966.

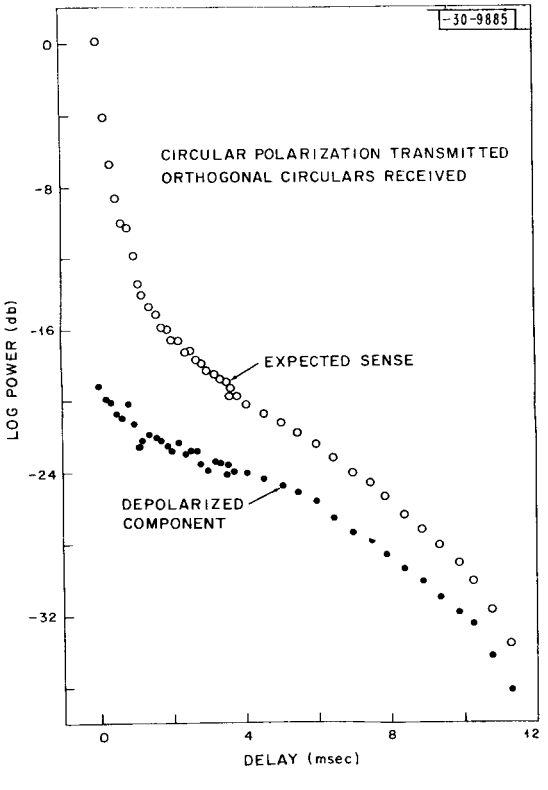

Fig. 7. Comparison of Fig. 6 results with a determination of the expected component of echo power (3 Feb. 1966).

power, P(t). In order to remove the effects of pulse length, P(t) was redetermined using a 160-μsec pulse and a 50-kcps receiver bandwidth. Figure 7 compares the curves obtained for the two polarizations. The percentage polarization p(t) which can be defined as

$$p(t) = \frac{P(t) - D(t)}{P(t) + D(t)} \times 100 \qquad (1)$$

is then plotted in Fig. 8. Also shown is the curve for p(t) obtained previously at 68 cm by Evans and Pettengill (1963b). It can be seen that the amount of depolarization has increased with frequency.

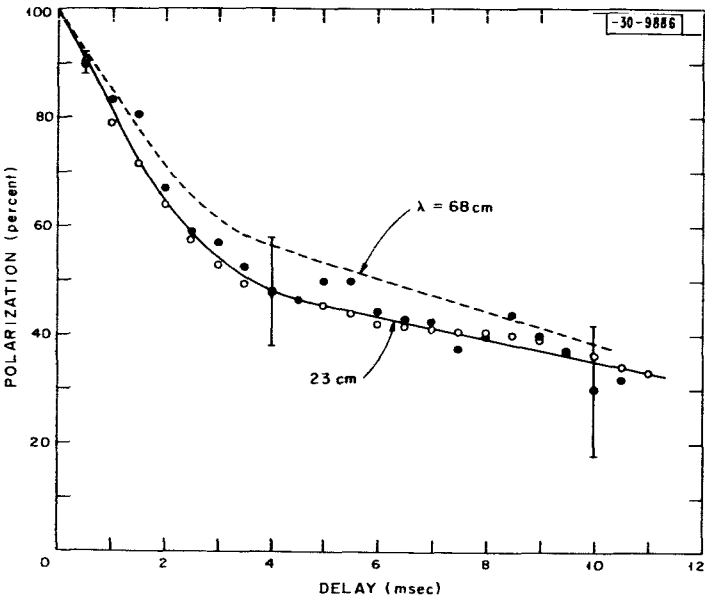

Fig. 8. Percentage polarization observed for circularly polarized components (Fig. 7) compared with previous results for 68 cm.

Two independent sets of measurements are included in deriving Fig. 8. The error bars indicate the uncertainty associated with the points shown as closed circles. The difficulty of establishing the exact relative position of the two curves in Fig. 7 is the major source of uncertainty in deriving percent polarization. To establish these curve positions as well as possible, it was necessary, in addition to including a calibration pulse in each measurement, to establish the waveguide and other losses between the horn feed and the receiver input terminals for the two senses of polarization. This was done using a beacon transmitter coupled to a dipole mounted on a tower in the near-field of the antenna. The dipole could be rotated at will without influencing the amount of power radiated by the beacon transmitter. In this way the circularity of the transmission and reception could be checked. The agreement between the two sets of points in Fig. 8 lends some confidence in the method and suggests that the uncertainty estimate that has been assigned is too large.

5. Observations of Total Radar Cross Section

Previous efforts to obtain reliable total cross section measurements for the moon have been reviewed by Evans and Pettengill (1963c). The errors encountered are usually large, because the uncertainty in the antenna gain (typically 1 db) enters twice, and uncertainties associated with the determination of the absolute power transmitted and the absolute calibration of the receiver are usually of comparable order.

A very precise determination of the moon's radar cross section is now possible by comparing the lunar echoes with those from a carefully machined metal sphere placed in earth orbit. This sphere, the Lincoln Calibration Sphere (LCS) has a cross section of exactly 1 m^2 at a wavelength of 23 cm (Prosser, 1965). Unfortunately, despite its close range the calibration sphere is a weaker target than the moon by approximately 40 db. Accordingly, the full sensitivity of the Millstone Hill radar is required in order to observe it accurately.

The procedure adopted in these measurements was as follows: A time was chosen when the moon's elevation and that of the sphere were comparable. The sphere was then tracked using the normal closed-loop tracking afforded by the multiple beam system of the Millstone Hill radar. The automatic tracking system requires the transmission of 2-msec radar pulses. A separate receiver with a bandwidth of 8 kcps was used in order to determine the echo amplitude. The output of this receiver was rectified using a square-law detector and sampled at 200-μsec intervals. The integration over the time-base was achieved by summing the digital samples in a computer for consecutive 30-second intervals. Included in the integration process was the normal calibration noise pulse. About forty successive 30-second integrations were obtained and each of these was used to determine the overall sensitivity of the radar using an appropriate value determined for the mean range of the satellite during that 30-second period. These observations yielded the following relation:

$$\log_{10} T_{echo} = 18.071 \pm 0.038 - 4 \log_{10} R \qquad (2)$$

where T_{echo} is the equivalent increase in the system temperature caused by the satellite echo and R is its range. Based upon the parameters of the radar system as determined from independent calibrations (Table II) we should expect

$$\log_{10} T_{echo} = 18.066 = 4 \log_{10} R \quad . \qquad (3)$$

In this instance it seems that the radar sensitivity could, in fact, have been quite accurately predicted without this overall calibration. The agreement between (2) and (3), however, lends considerable confidence to the result reported here. There is still no way of being certain of the values of individual equipment parameters to better than ±1 or 2 db.

Following the observations of the LCS sphere, the radar was employed to observe the moon in precisely the same way, except that the antenna pointing information was derived from the punched paper tape reader. Since the moon echoes are very much stronger than those from the satellite, it was also necessary to reduce the system sensitivity by about 30 db to prevent the receiver from saturating. This was accomplished by reducing the transmitter power by an amount which was measured using a carefully calibrated power meter. It is also possible to achieve the same effect by placing attenuators at the receiver input terminals, but this was

considered undesirable as it could disturb the matching of the receiver to the line. The choice of an 8-kcps receiver bandwidth was made in order to remove any amplitude fluctuations that might arise from small errors in the automatic compensation of the Doppler shift during the observations of the calibration sphere. Observations of moon echoes were made for periods of 30 seconds and a mean of 14 such periods was then taken. Since a 2-msec pulse is less than the full depth of the moon (11.6 msec), at no time was the whole lunar hemisphere illuminated and therefore contributing to the echo power. That is, the cross section $\sigma(T)$ observed with a pulse length of T milliseconds, is simply

$$\sigma(T) = \frac{\sigma_o \int_o^T P(t)\,dt}{\int_o^{11.6} P(t)\,dt} \tag{4}$$

where σ_o is the total cross section. This function is plotted in Fig. 9. When the cross section observed with 2-msec pulses is scaled up to the value for the whole moon we obtain

$$\sigma_o = 0.065 \pm 0.008\ \pi a^2 \quad . \tag{5}$$

where a is the moon radius. The uncertainty given is the rms error resulting from the spread of the values obtained in the 40 observations of the satellite (±0.38 db) and the 14 observations of the moon (also ±0.38 db). We believe that the only source of systematic error remaining is that associated with reading the power meter monitoring the transmitter power and the linearity of its scale. These errors are thought to be substantially smaller than the uncertainty quoted.

6. Discussion of Results

The wavelength dependence in the scattering behavior reported initially by Evans and Pettengill (1963b) and supported by Davis and Rohlfs (1964) and Klemperer (1965) is strengthened

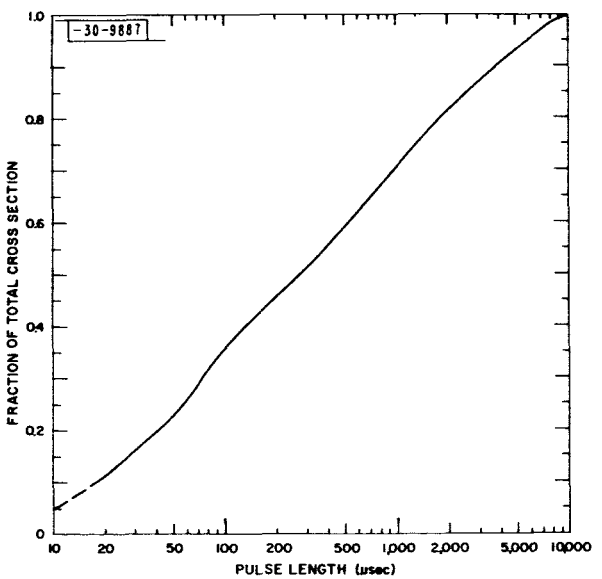

Fig. 9. Variation of total cross section of moon at 23 cm wavelength as a function of pulse length. Curve was derived from results presented in Fig. 4 and has been employed in obtaining an accurate determination of radar cross section of moon (Sec. I-A-5).

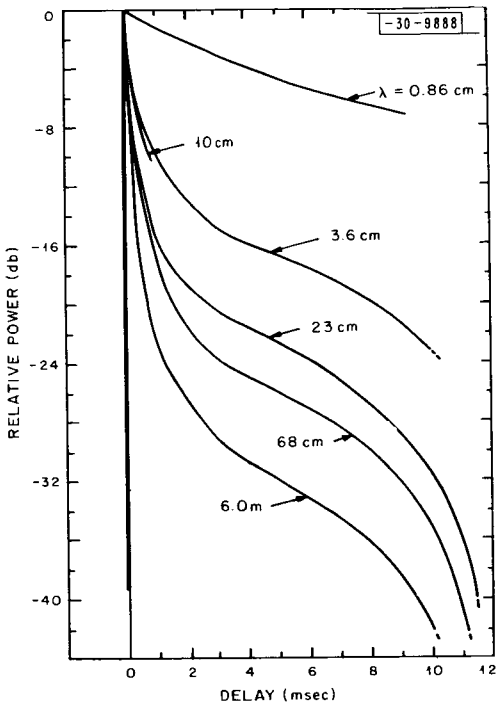

Fig. 10. Summary of radar observations of moon using pulse length of 100 μsec or less.

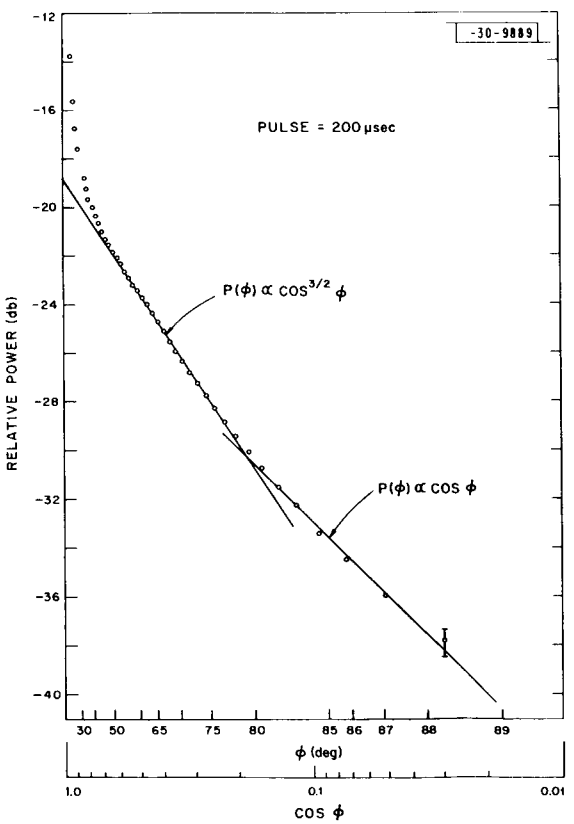

Fig. 11. Results obtained for expected echo component (Fig.2) replotted as a function of cos φ at 23-cm wavelength.

by these observations. Figure 10 shows all the observations made to date in which a pulse length of 100-μsec or less was employed. That is, Fig. 10 contains the results of all the observations listed in Table I except those of Davis and Rohlfs (1964). The results have been normalized at the origin, but since the resolution achieved in this region varied, it is likely that the absolute relationship between the curves shown in Fig. 10 is slightly in error. In spite of this the wavelength dependence in the results is readily apparent. This behavior must mean that there is a continuum of structure on the lunar surface (or perhaps within the upper layer) having scales in the range of wavelengths that have been employed.

Since there is a direct relation between the echo delay t and the angle of incidence φ between the ray and mean surface normal, the angular dependence of the echo power per unit surface area $P(\varphi)$ can be examined simply by replotting the echo power as a function of φ. In Fig. 11 we have plotted these 23-cm results as a function of log cos φ to test whether a law of the form

$$P(\varphi) \propto \cos^n \varphi \tag{6}$$

fits the data. The case for the exponent n = 1 would indicate a uniformly bright surface since a pulse of fixed length illuminates a region whose projected area falls as cos φ. The case n = 2 would indicate a Lambert law surface. The results shown in Fig. 11 indicate that the region $80° < \varphi < 90°$ is uniformly bright (n = 1), but that in the range $50° < \varphi < 80°$ the law

$$P(\varphi) \propto \cos^{3/2} \varphi \tag{7}$$

is encountered. The behavior shown in Fig. 11 is essentially similar to that reported by Evans and Pettengill (1963b) at 68 cm.

No adequate explanation has yet been found for the law [Eq. (7)] which lies midway between uniformly bright and Lambert scattering. However, since the surface is nearly uniformly bright we are forced to suppose that the scatterers are nearly isotropic reflectors. Small scale elements having vertical and horizontal dimensions of comparable or smaller size than the wavelength would behave in this fashion. Evans and Pettengill (1963b) argued on this basis that the regions obeying the linear relations plotted in Fig. 11 are those in which the small scale elements of the surface scatter more strongly than the smoother portions – probably because few large elements of the surface are inclined at such large angles to the mean surface. This region (i.e., $\varphi \geqslant 40°$) was termed "diffuse." For $\varphi < 40°$ the scattering appears very sensitive to the angle of incidence and hence is attributed to the smoother undulating portions of the surface which can be treated as flat facets. This scattering has been called quasi-specular.

The division of the echo power into two regions attributable to two broad classes of surface structure has been encountered at all the radio wavelengths employed thus far. Figure 12 shows the results given in Fig. 10 when replotted as a function of 1 + log cos φ. We find that beyond 4 msec ($\varphi \sim 50°$) delay all the curves in Fig. 12 become straight lines indicating that the law (Eq. 6) holds. For wavelengths of 600, 68 and 23 cm the exponent n [Eq. (6)] is found to be n = 3/2 and for 3.6 and 0.86 cm it appears to be near unity, though here the results are somewhat less certain.

We note that though some authors (e.g., Daniels, 1963a, b; Rea, et al., 1964) have accepted the interpretation of the curves (e.g., Fig. 11) in terms of two classes of scatterers, others

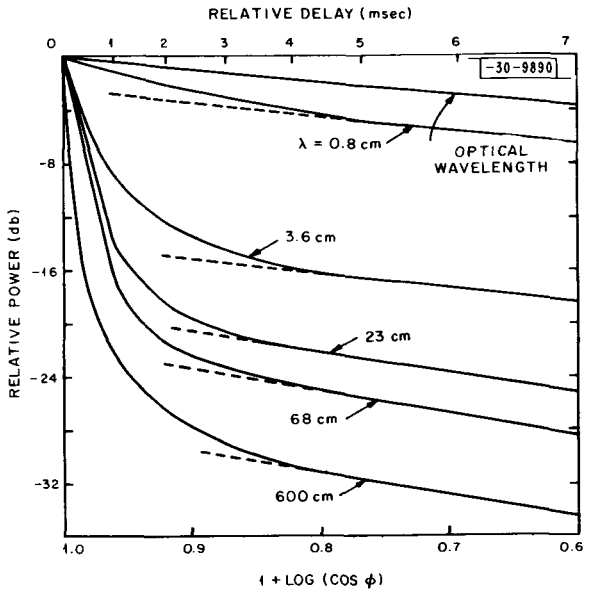

Fig. 12. Results shown in Fig. 10 replotted as a function of 1 + log cos ϕ.

(e.g., Muhleman, 1964; Beckmann, 1965b) have not, and instead have attempted to explain the complete curve $P(\varphi)$ in terms of quasi-specular scattering. This requires that there be substantial amounts of surface area tilted at very large angles to the mean surface and the rms slope one derives as a result is correspondingly large. We do not think that this view is correct and have argued against it previously (Evans and Hagfors, 1964). Further evidence in support of the model outlined above is available from the work of Katz (1965) who has considered the wavelength dependence of the absolute echo power at given delays. Katz finds that near the leading edge the cross section per unit area increases with wavelength, whereas in the diffuse tail the cross section per unit area vs wavelength has a negative dependence, implying a different scattering mechanism. A similar conclusion has been reached by Peake and Taylor (1963) who compared the results reported by Evans and Pettengill (1963b) with scattering from different types of terrestrial surface. We shall return to this point when discussing the polarization results.

The amount of power associated with the diffuse component of the echoes is listed in Table III.

TABLE III
PERCENT OF TOTAL POWER IN DIFFUSE COMPONENT

λ(cm)	Percent
68	20
23	25
3.6	35
0.86	85

When the diffuse component of the power, i.e., that corresponding to the straight lines in Fig. 12, has been subtracted, the remainder observed at 3.6, 23 and 68 cm appears as plotted in Fig. 13. This component of the power is related to the distribution of surface slopes and will be discussed further below. We have been unable to find any simple empirical law to describe this component, which, by adjusting a single constant, will match the results at all wavelengths. Evans and Pettengill proposed a law of the form $P(\varphi) \propto (1 + b\,\varphi^2)^{-1}$, but a more careful computation of the power in the quasi-specular component (presented in Fig. 13) shows that this law is inexact. Good agreement can be obtained with a law published by Hagfors (1964) that has been derived from theoretical considerations.

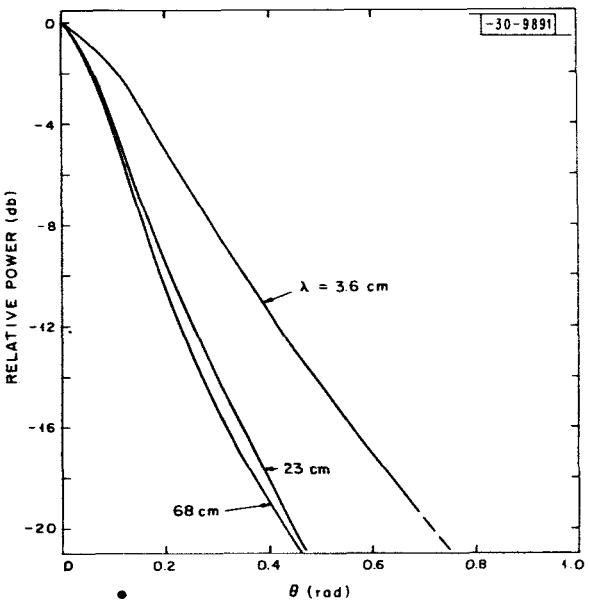

Fig. 13. Quasi-specular component of echoes. Small difference between results at $\lambda = 23$ and $\lambda = 68$ cm indicates that at these two wavelengths the distribution of surface slopes appears to be about the same.

The measurements reported above for the depolarized component are open to at least two possible types of explanation, namely, (a) some elements of the surface may have small radii of curvature and as such can act as dipoles, and (b) the reflection coefficient may depend upon the relation between the plane of polarization and local plane of incidence. Thus, for example, multiple reflections may occur, one of which is near the Brewster angle, or the echo may be partly reflected from within the lunar surface and hence depend upon the transmission coefficient of the uppermost layer.

Evans and Pettengill (1963b) attributed the depolarization to effect (a). Hagfors, et al. (1965) have shown, however, that for $\varphi > 40°$ it appears that the echo is entirely reflected from within the lunar surface and thus the echo power from any small region depends upon the square of the local transmission coefficient. Since the transmission coefficients for waves polarized in and normal to the local plane of incidence are different, and any one range ring includes all possible local planes of incidence, this will serve to cause some depolarization. However, it appears that the magnitude of an effect of this type is inadequate to account for the large amount of depolarization observed as shown in Fig. 7. Stated otherwise, although an effect of type (b) is demonstrably present in lunar reflection, the original explanation (a) proposed by Evans and

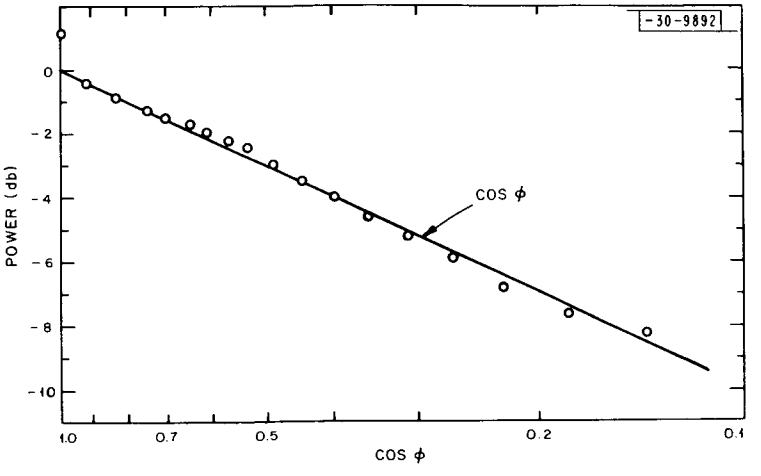

Fig. 14. The angular scattering law for the depolarized component of echoes D(t) plotted in Fig. 6 (3 Feb. 1966).

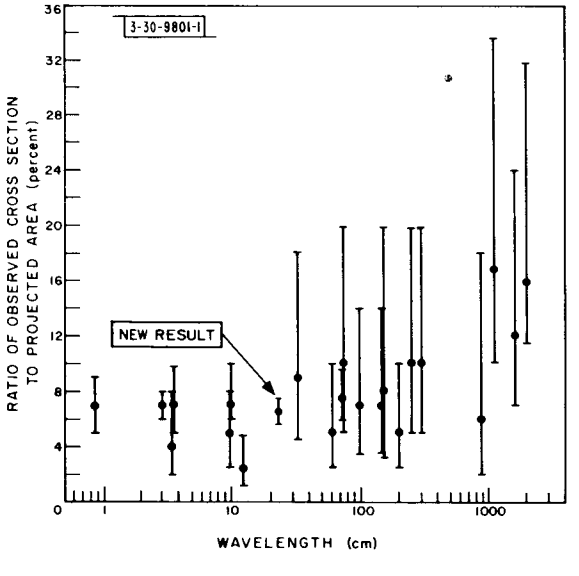

Fig. 15. Cross section of moon vs wavelength with new result added.

Pettengill (1963b) appears correct. We note that Long (1965) invokes a similar explanation in attempting to account for the polarization of radar echoes from the sea at grazing incidence.

The echoes from the quasi-specular region are not depolarized much and this is to be expected for reflections from a largely smooth undulating surface (Hagfors, 1964). There is, however, a marked transition at about 3-msec delay (Fig. 8) beyond which the amount of depolarization is roughly constant. We may model the scatterers in this region as flat facets which do not depolarize and a random collection of linear dipoles which do. Randomly arranged dipoles would completely depolarize an incident circularly polarized wave, since they would destroy the $\lambda/4$ phase relationship between the two linears into which a circular wave may be resolved. Thus in order to account for the amount of polarization (about 40 percent) observed at t = 8 msec (Fig. 8) we require that roughly 40 percent of the energy be returned from the facets and 60 percent from the dipoles. In this case the dipoles will split their reflections equally between the two components to give 30 percent in the depolarized component and 70 percent will appear in the expected sense – as is observed. When linearly polarized waves are employed the dipoles reflect in the incident and orthogonal planes in the ratio 3:1 (Mack and Reiffen, 1964). It follows that of the 60 percent of the power reflected by the dipoles, only 1/4, i.e., 15 percent, will be in a sense orthogonal to the expected mode. We should be ready to report a comparison of this prediction in the next quarterly progress report.

Some support for the model proposed here is given in Fig. 14 where we have plotted the echo power observed in the opposite sense circular mode to the expected sense [i.e., D(t) shown in Fig. 6] as a function of $\cos\varphi$. We find that the echo power conforms to the law $D(\varphi) \propto \cos\varphi$, which is similar to the law observed for the diffuse component of the expected signal in the extreme limb region. A law $D(\varphi) \propto \cos\varphi$ was also observed at 68 cm (Evans and Pettengill, 1963b).

It should be understood that this modeling of the surface as a collection of facets and dipoles is merely a convenient fiction which approximately serves to describe the electrical performance of the surface. We do not suppose that the lunar surface is covered with dipoles, but merely that there are elements having small radii of curvature and as such force the induced currents to flow in preferred directions different from those of the field exciting them. These results support the view advanced earlier that the scattering in the diffuse region is dissimilar to that of the center of the disk.

Let us now turn to the significance of the new and accurate determination of total cross section reported above. Previously obtained data were presented in QPR (1966:1) as Table II in terms of fractions of physical cross section. The data were also presented as Fig. 3 of that report which is reproduced here, with the new, accurate 23-cm value added, as Fig. 15. The increase in cross section with increasing wavelength suggested depends largely on the three long wave measurements reported by Davis and Rohlfs (1964). These measurements may have been subject to systematic errors introduced by ionospheric effects. If these three points are ignored, the remainder show no clear wavelength dependence. The errors given are the reported values where these have been given, or ±3 db where no uncertainty was published.

The errors associated with these measurements are generally large for reasons we have already enumerated. It seems that a reliable determination of the cross section vs wavelength would require that each radar be calibrated in the manner described in Sec. A-5.

The scattering cross section expected for a large dielectric sphere may be written (Evans and Pettengill, 1963b)

$$\sigma_o = g\rho_o \pi a^2 \tag{8}$$

where ρ_o is the Fresnel reflection coefficient for normal incidence and g a term which denotes the directivity of the target, i.e., the ability to scatter preferentially toward the radar. In the case of a perfect sphere g = 1 and for the case where the surface has large scale irregularities (but is locally smooth on the scale of at least a wavelength) $g = 1 + \alpha^2$, where α^2 is the mean square surface slope (Hagfors, 1964). For the general case in which the sphere is covered with a range of structure having scales down to and smaller than the wavelength in size, g has not been evaluated quantitatively. If the surface is completely covered with structure comparable with the wavelength and as a result behaves as a Lambert scatterer, then g = 8/3 (Grieg, et al., 1948). It is thought, therefore, that as the surface is covered to an increasing extent with objects comparable in size to the wavelength, g increases from unity toward a value of about 3 or possibly higher.

For the long wave measurements ($\lambda \geq 1$ m) shown in Fig. 3 of QPR (1966:1) we conclude that $g \approx 1.0$ but that g increases for $\lambda < 1$ m. The absence of a corresponding increase in σ_o indicates that ρ_o is decreasing with wavelength, and hence suggests that the reflection arises in an inhomogeneous surface. If the density of the material on the lunar surface increases with depth then the longest waves will penetrate deepest and the effective reflection coefficient will increase accordingly.

From the 68-cm results Evans and Pettengill (1963b) derived a reflection coefficient $\rho_o = 0.064$ after attempting to subtract out the echo power attributable to the diffuse component. By assuming that the electrical conductivity of the lunar surface is zero and hence the dielectric constant $k = (1 + \sqrt{\rho_o})^2/(1 - \sqrt{\rho_o})^2$ Evans and Pettengill derived a value k = 2.8. Rea, et al. (1964) used the same experimental results, but employed a somewhat more rigorous method of removing the echo power attributable to the rough structure (for which the value of g is not known) and obtained k = 2.6. These radar values, although very low when compared with the values observed for terrestrial rocks (Brunschwig, et al., 1960) are in fact considerably higher than values obtained in passive radiometric observations. Perhaps the most reliable method of deriving k in such studies is to determine the degree of polarization exhibited by the thermal radio emission, since this depends directly upon the transmission coefficient of the surface $(1 - \rho_o)$ (Troitsky, 1954). Measurements of this kind have been performed by a number of observers (e.g., Soboleva, 1962; Heiles and Drake, 1963; Mezger, 1965; Davies and Gardner, 1965) and yield values chiefly in the range k = 1.7 to k = 2.1. Other values obtained by studying the thermal history of the moon over a lunation are less direct but also yield values in the range 1.5 to 2.0 (e.g., Troitsky, 1962; Salomonovich and Losovsky, 1962; Krotikov and Troitsky, 1962). The discrepancy between the radar and passive results has long remained a puzzle. Calculations (Hagfors and Morriello, 1965) of the effect of surface roughness on the interpretation of the passive observations have indicated that, though this does tend to raise the value of k that is derived, the effect is not large enough to account for the discrepancy. The difficulty seems resolved as a result of recent radar observations reported by Hagfors, et al. (1965) which

indicate that the radar echoes at normal incidence are partially reflected from within the lunar surface, and that the upper layer has a dielectric constant of only about 1.8. (For further details see QPR (1966:1) Sec. I-J.) It seems, therefore, that the passive measurements refer to the uppermost material (extending in depth perhaps some tens of centimeters) and that the radar reflections yield an average value related somehow to the way in which the density increases as a function of depth.

Giraud (1965) has examined the way in which the reflection coefficient would vary in the case of a surface in which the density increases from zero linearly with depth over a distance of d to a density corresponding to a dielectric constant k_1. On the basis of this model, it is only when $\lambda > 20$ d that the reflection coefficient is the same as that which would be attributed to the subsurface layer in the absence of an inhomogeneous covering. If the measurements listed in QPR (1966:1) Table II could be repeated with an accuracy equal to that reported in this paper, it seems that the depth of the layer of light material overlying the lunar surface might be established. Further discussions of possibilities for determining the depth of a surface layer on the moon are given in Sec. III-A.

7. Conclusions

On the basis of the experimental results presented in this section it is possible to draw a number of conclusions about the behavior of the lunar surface as a whole as a scatterer of radio waves. The wavelength dependence observed by earlier workers has been supported by these measurements. By employing different polarizations for transmission and reception, some of the depolarizing properties have been explored. These results support the view that the scattering from the center of the disk is largely from regions that are locally smooth on the scale of the wavelength, whereas for an angle of incidence $\varphi > 40°$, scattering from rough structure appears to predominate. In the central region the theory of the scattering apparently is in satisfactory shape, and the surface can be described as having an exponential autocorrelation function and a mean slope of about 10° when measured over an interval of a few meters. In the limb region where scattering from rough structure predominates the theory is less satisfactory. The scatterers may be modeled as collections of dipoles and flat facets, and at 23-cm wavelength 60 percent of the power is reflected by the dipoles. This irregular structure appears, however, to lie largely within the surface according to separate experiments reported by Hagfors, et al. (1965). The depth and perhaps some other properties of the uppermost tenuous layer might be inferred if very precise radar cross section measurements could be made at many wavelengths. Section A-5 outlines one method of accomplishing this using a precisely machined calibration sphere in Earth orbit as a radar reference standard.

B. OTHER OBSERVATIONS

In this section a brief review is given of some additional observations made during this reporting period, most of which are still being analyzed. Results must, therefore, be regarded as tentative.

1. Polarization Observations at 23-cm Wavelength

Some additional polarization experiments have been carried out at 23-cm in order to obtain further information on the nature of the scattering mechanism involved, particularly in the limb regions of the surface.

The moon was illuminated by linearly polarized waves and the behavior of the polarized and the depolarized linear components was studied for returns from complete range rings. The behavior of the polarized component appears to be the same as that of the polarized component when the illumination is circularly polarized. The depolarized component, however, behaves somewhat differently from the one observed when the illumination is circularly polarized. The angular scattering law appears to follow a $\cos^{3/2}\varphi$ law rather than a $\cos\varphi$ law as in the circular polarization case, for reasons not fully understood at present. The ratio of polarized to depolarized components in this case appears to remain approximately constant at 6 to 7 db from a delay of 3 msec on out to the lunar limb.

Further studies were conducted with linearly polarized illumination with small areas resolved by means of the range-Doppler technique. Results show that with the illuminating wave polarized with the E-field in the plane of incidence, the ratio of depolarized to polarized received components increases out to 3-msec delay, then remains constant to about 8 msec as for the return from a complete range ring. Beyond 8 msec, however, the ratio starts decreasing again toward the limb at 11.6 msec where it is only approximately 50 percent of its value when a range ring is considered as a whole. This behavior appears to confirm the results of previous polarization experiments conducted by Hagfors, et al. (1965).

2. Observations at a Wavelength of 3.8 cm

Work on the series beam-switch regulator (SBSR) and other hardware was completed at Haystack during the quarter, so that short pulse radar observations became possible. This new capability was used to make two different types of observation, namely measurement of the mean scattering law of the moon at a wavelength of 3.8 cm and measurement of the ratio of the back-scattering coefficients for the two orthogonal linearly polarized components, one aligned with the plane of incidence, the other orthogonal to this plane.

The determination of the mean scattering law was carried out by measuring the power as a function of range for a number of different offsets of the center of the antenna beam from the sub-radar point. The experiment was performed by offsetting the antenna beam in steps along several radii across the lunar disk. Accurate knowledge of the effect of the antenna polar diagram makes it possible to determine the angular scattering law within certain angular intervals for each antenna offset. The results thus obtained may be joined together to make a complete power vs angle plot for the entire range of angles from normal incidence to grazing incidence. The information contained in these data should provide a mean scattering law against which the lunar maps to be obtained somewhat later in this program may be compared. The analysis of the large amount of data obtained has not yet been completed, but the mean lunar scattering law at this wavelength should be available for the next Quarterly Progress Report.

The polarization experiment was carried out in a way similar to the 23-cm experiment reported in QPR (1966:1). The illumination was circularly polarized. Two receiver channels were

used to receive orthogonal linear polarizations. The direction of linear polarization of one of the two channels was always adjusted to be aligned with the radius connecting the beam center and the center of the lunar disc. In this way one channel would always correspond to one having its E-field aligned with the plane of incidence. The angular discrimination required to single out the limited areas necessary was achieved by range gating and by the limited angular extent of the polar diagram of the antenna beam. Preliminary analysis of the data has shown that the scattering is stronger for the component that is polarized (E-field) in the local plane of incidence, which was also the case at L-band (Hagfors, et al., 1965). The ratio of the two backscattering coefficients at 3.8 cm is, however, significantly closer to unity than at 23 cm. The interpretation of this result is not yet clear. It may be related to a gradual increase in dielectric constant with depth, with the assumption that the backscattering takes place from irregularities embedded in the surface layer. It may also be that small scale irregularities – small pebbles – are present on top of the surface to cause appreciable scattering at 3.8 cm but negligible scattering at 23 cm. Further study of the results is required.

C. THEORETICAL RESULTS

1. The Effect of Shadowing on the Backscattering of Waves from a Random Rough Surface

As was explained in QPR (1966:1) the scattering from the lunar surface can be described in terms of an exponential correlation function relating neighboring height-deviations on the surface. This description holds only for the so-called quasi-specular component which is dominant out to an angle of incidence of 30 to 40°, depending on wavelength.

Beckmann (1965a) recently advanced a theory to account for the shadowing effect and was able to predict quite accurately the scattering law of the moon on the basis of his theory (Beckmann, 1965b). Because it was felt that some of the physical principles underlying Beckmann's approach were invalid, some work was started to check the theory of the shadowing.

In Beckmann's shadowing theory as applied to lunar and planetary radar returns the scattered power is first determined without respect to shadowing, and then the shadowing is taken into account by multiplying this result by a function $S(\Theta)$ which is basically the fraction of the total surface still illuminated, and which varies from unity at normal incidence ($\Theta = 0$) to zero at grazing incidence ($\Theta = 90°$).

For the case of a random rough surface which introduces "deep" phase modulation in the scattered wave, it is well known (Hagfors, 1964) that the scattering in this type of approach takes place mainly from areas which are oriented so as to provide specular reflection in the direction of the observer. Thus, in the backscattering case, only surface elements which are perpendicular to the line of sight of the observer will contribute significantly. The effect of shadowing, it seems, should therefore not be a question of the fraction of illuminated area, but rather a question of the fraction of illuminated, favorably oriented surface elements. Intuitively, in backscattering, it seems that a potential reflection point is much less likely to be in the shadow than an arbitrary point on the surface. It was therefore felt that the "shadowing theory" would overestimate the effect of shadowing by a considerable amount.

In order to justify that the number of favorably oriented reflection points per unit surface area (per unit length in a convenient one-dimensional surface model) is indeed proportional to

the backscattered power, we have to show first that this leads to the correct result in the geometric optics limit. In this limit the amount of power returned from a specular point is proportional to the radius of curvature at that point.

Let the surface height deviations from a plane mean surface be described by the function f(x), where x is the distance along the mean plane in the plane of incidence. Let ℓ be the total extent of the surface and let ℓ_S be the extent of the total surface which is in the geometric shadow. Beckmann's shadowing function is then defined as:

$$S(\Theta) = (\ell - \ell_S)/\ell \quad . \tag{9}$$

Let the number of points on the surface which have a normal along the line-of-sight to the observer be N_R and let the number of these which are in the geometric shadow be N_{RS}. The shadowing function which we believe is correct is defined by:

$$R(\Theta) = (N_R - N_{RS})/N_R \quad . \tag{10}$$

In order to show that $R(\Theta)$ is the strictly correct solution in the limiting case of geometric optics it is only necessary to show that the mean backscattered power is exclusively determined by the probability distribution of surface slopes. This can be shown quite readily following the method of Kac (1943). Introduce the following variables:

$$\xi = \frac{df}{dx} \quad ; \quad \eta = \frac{d^2f}{dx^2} \quad . \tag{11}$$

Let the joint probability density of ξ and η at a point $x = x_1$ be denoted by $p(\xi, \eta; x_1)$. The probability that ξ crosses the level $\xi = \tan\Theta$ (i.e., condition for reflection point) with $\eta_1 < \eta < \eta_1 + d\eta$ is:

$$d\eta \cdot |\eta_1| \; p(\tan\Theta, \eta_1; x_1)\, dx \quad . \tag{12}$$

When reflection occurs at an angle of incidence Θ from a point where $d^2f/dx^2 = \eta_1$, the contribution to the power in the limit of geometric optics is proportional to $\cos^{-3}\Theta \cdot |\eta|^{-1}$, i.e., to the inverse of the magnitude of the radius of curvature at that point. The mean contribution to the backscattered power at an angle of incidence Θ from the interval x_1, $x_1 + dx$ is, therefore:

$$dP \sim dx \cos^{-3}\Theta \int_{-\infty}^{+\infty} p(\tan\Theta, \eta; x_1)\, d\eta = \cos^{-3}\Theta \; p(\tan\Theta; x_1)\, dx \quad . \tag{13}$$

The backscattered power per unit area (length) is therefore seen to be purely a matter of surface slope. In the numerical analysis presented below we essentially determine $p(\tan\Theta; x_1)$ for the cases when x_1 is an arbitrary point on the surface and when x_1 is a point in the shadow. In other words we determine:

$$p(\tan\Theta; \text{ arbitrary}) = \frac{N_R}{\ell}$$

$$p(\tan\Theta; \text{ shadow}) = \frac{N_{RS}}{\ell_S} \quad . \tag{14}$$

Our shadowing function $R(\Theta)$ as defined in (10) can be rewritten as:

$$R(\Theta) = (N_R - N_{RS})/N_R = \left[\ell\left(\frac{N_R}{N}\right) - \ell_S\left(\frac{N_{RS}}{N_S}\right)\right]\Big/\ell \cdot \left(\frac{N_R}{N}\right)$$

$$= (\ell \cdot p(\tan\Theta;\ \text{arbitrary}) - \ell_S \cdot p(\tan\Theta;\ \text{shadow}))/\ell$$

$$\cdot\ p(\tan\Theta;\ \text{arbitrary}) \qquad (15)$$

It can be seen that our $R(\Theta)$ is identical to $S(\Theta)$ only under the condition that

$$p(\tan\Theta;\ \text{shadow}) = p(\tan\Theta;\ \text{arbitrary}) \quad . \qquad (16)$$

Several vain attempts were made to obtain an analytical evaluation of the fraction of reflection points in shadow. This approach was finally abandoned and instead a digital computer experiment was devised to compare Beckmann's shadowing function with the relative number of illuminated reflection points.

Random uncorrelated noise samples were obtained by sampling receiver noise by means of an analog-to-digital converter. The center frequency of the IF noise output was 200 kcps and the bandwidth was 100 kcps. The rate of sampling was 25 kcps and the time taken to estimate each sample was about 50 nanosec. The rms value of the noise was about 0.25 volt, and the peak to peak range of the analog to digital converter was 3 volts. This three-volt range was quantized into 64 levels corresponding to six bit numbers. The resulting uncorrelated noise samples were stored on a magnetic tape for further analysis.

From these noise samples a sequence of correlated noise samples can be generated by filtering in a computer. This filtering process can be expressed by the following sum

$$f_i = \sum_{j=-N}^{+N} w_j\, n_{j+i} \qquad (17)$$

where w_j are weight factors determined by the type of autocorrelation function desired for f_i, and where n_j is one of the uncorrelated noise samples. It can be shown that the autocorrelation function of the w_j must be made identical to the one desired for f_i. For the sake of illustration we consider here only the case of a gaussian autocorrelation function for the surface. The weight factors must then also be gaussian with a "width" which is $1/\sqrt{2}$ of that of the desired autocorrelation function. The sum in (17) which should be carried between infinite limits was truncated by putting $N = 50$. The weight factors w_j were chosen from tables of the function $\exp(-x^2) \cdot 2/\sqrt{\pi}$ (Gautschi, 1964) as follows:

$$w_j = \frac{2}{\sqrt{\pi}} \exp\left[-(j/20)^2\right] \quad . \qquad (18)$$

The autocorrelation function of f_i should hence fall to e^{-1} for a shift of $20 \times \sqrt{2} \approx 28$ points. A magnetic tape was produced by means of the formula (17) with the weight factors (18). A total number of 1,290,600 correlated noise samples was produced and stored. As a check on the correlated noise tape the autocorrelation function was computed for different sections of the

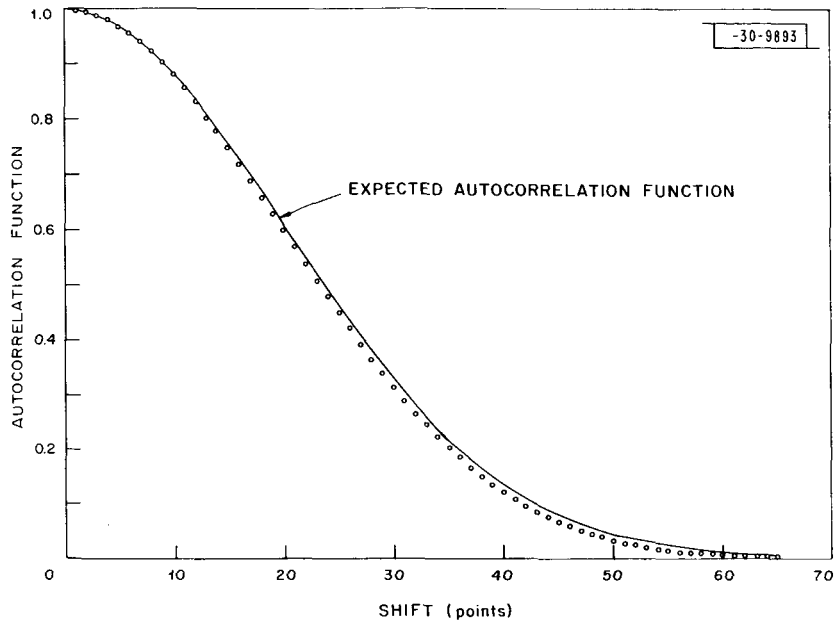

Fig. 16. Comparison of computed and desired autocorrelation functions for surface model.

noise tape to test for stationarity. The autocorrelation function found for the first 648,885 samples is shown in Fig. 16 and is compared with the expected autocorrelation function $\exp[-(1/2)(i/20)^2]$. As can be seen, the autocorrelation estimated very closely fits the expected value. The fact that the computed autocorrelation function is slightly narrower than the expected one obviously stems from the truncation in the sum (17).

The actual computational procedure used to arrive at the relative area shaded, the number of reflection points and the number of reflection points lost in the shadowed regions is best explained with reference to Fig. 17. The beginning of a region of shadow between sampling points i and i − 1 is characterized by the condition:

$$\left(\operatorname{cotan}\Theta + \frac{df_i}{dx}\right)\left(\operatorname{cotan}\Theta + \frac{df_{i-1}}{dx}\right) < 0 \tag{19}$$

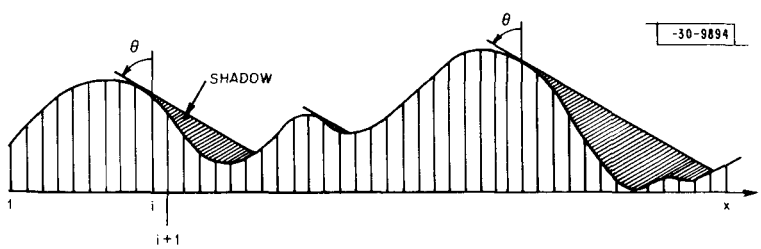

Fig. 17. Surface model, definition of angle of incidence, representation of shadowed regions.

where Θ is the angle of incidence and where f(x) is the noise-waveform from which the correlated samples are derived. The derivatives involved were actually computed from the samples by:

$$\frac{df_i}{dx} = (f_{i+1} - f_{i-1})/2\,\Delta x \tag{20}$$

where Δx is the spacing corresponding to subsequent samples.

When condition (19) is satisfied for $i = k$ and f_k is not already in the shadow a sequence of points is computed from the straight line formula:

$$C = f_k - (i - k)\,\Delta x \cdot \operatorname{cotan}\Theta \tag{21}$$

and a test is made to determine whether the points following point k lie above or below this straight line. Whenever $f_i < C$ the count of points in shadow is increased by one. Let this number be denoted by N_S. As soon as $f_i > C$, the search for a starting point for another tangent is reinitiated. By counting the total number of points in the shadow and dividing by the total number of samples in the sequence an estimate of the fraction of the surface in the shadow is obtained. This should correspond to the shadowing function of Beckmann (1965a).

At the same time a test is carried out to determine reflection points. These are characterized by the condition:

$$\left(\tan\Theta - \frac{df_i}{dx}\right)\left(\tan\Theta - \frac{df_{i-1}}{dx}\right) < 0 \tag{22}$$

and corresponds to the incident ray being perpendicular to the surface somewhere in the interval between $(i - 1)\,\Delta x$ and $i\,\Delta x$. The total number of such points is counted and denoted by N_R and the number of such points which are also in the shadow is counted separately and denoted by N_{RS}. If the total number of samples analyzed is N, the required shadowing functions are defined by:

$$S(\Theta) = (N - N_S)/N \tag{23}$$

corresponding to Beckmann's theory and:

$$R(\Theta) = (N_R - N_{RS})/N_R \tag{10}$$

corresponding to what we believe to be the more appropriate shadowing function.

The rms value h_o of all the f_i on the correlated noise tape was found to be 0.1296247 and the numerical value for Δx was chosen so that the ratio L/h_o assumed the values 1, 2, 4 and 10. The quantity L is the scale length in the gaussian autocorrelation function:

$$p(\delta x) = \exp[-(\delta x/L)^2] \quad . \tag{24}$$

In view of the discussion in the previous section, we see that $L = 28\,\Delta x$ and hence that:

$$\frac{L}{h_o} = \frac{28\,\Delta x}{0.1296247} \quad . \tag{25}$$

The numerical results of the computations are given in Tables IV, V, VI and VII. As a check on the computational results, N_R was normalized and plotted as a function of angle of incidence Θ.

TABLE IV

RESULTS OF NUMERICAL COMPUTATIONS
FOR $\Delta x = 0.004630$ AND $L/h_o = 1.0$

θ°	N_S	N_{RS}	N_R	S(θ)	R(θ)
5	0	0	35544	1.000	1.000
10	0	0	35286	1.000	1.000
15	8501	3	34952	0.993	1.000
20	52333	202	34427	0.959	0.994
25	130993	923	33817	0.899	0.973
30	224411	2194	32815	0.826	0.933
35	320853	3591	31566	0.751	0.886
40	415797	4860	29968	0.678	0.838
45	506752	5802	27890	0.607	0.792
50	594407	6391	24872	0.539	0.743
55	680416	6608	21390	0.473	0.691
60	763548	6079	16784	0.408	0.638
65	847261	4735	11140	0.344	0.575
70	930256	2567	5366	0.279	0.522
75	1013496	599	1056	0.215	0.433
80	1098711	7	10	0.149	0.300
85	1190228	0	0	0.078	–

TABLE V

RESULTS OF NUMERICAL COMPUTATIONS
FOR $\Delta x = 0.009259$ AND $L/h_o = 2.0$

$\theta°$	N_S	N_{RS}	N_R	$S(\theta)$	$R(\theta)$
5	0	0	24781	1.000	1.000
10	0	0	24189	1.000	1.000
15	0	0	23331	1.000	1.000
20	22	0	21936	1.000	1.000
25	1748	0	20202	0.998	1.000
30	10614	2	17888	0.988	1.000
35	31040	19	15396	0.966	0.999
40	66380	70	12350	0.927	0.994
45	113992	144	9078	0.874	0.984
50	170538	191	6046	0.811	0.968
55	235080	189	3354	0.740	0.944
60	305285	114	1300	0.662	0.912
65	382209	28	234	0.577	0.880
70	466631	4	16	0.483	0.750
75	558407	0	0	0.382	–
80	659741	0	0	0.270	–
85	771208	0	0	0.146	–

TABLE VI

RESULTS OF NUMERICAL COMPUTATIONS
FOR $\Delta x = 0.018519$ AND $L/h_o = 4.0$

$\theta°$	N_S	N_{RS}	N_R	$S(\theta)$	$R(\theta)$
5	0	0	34569	1.000	1.000
10	0	0	31506	1.000	1.000
15	0	0	26798	1.000	1.000
20	0	0	20942	1.000	1.000
25	0	0	14710	1.000	1.000
30	0	0	9206	1.000	1.000
35	0	0	4988	1.000	1.000
40	682	0	2076	0.994	1.000
45	4729	0	616	0.996	1.000
50	17827	0	112	0.986	1.000
55	47818	0	10	0.963	1.000
60	103513	0	0	0.920	–
65	189903	0	0	0.853	–
70	311074	0	0	0.759	–
75	471181	0	0	0.634	–
80	677102	0	0	0.475	–
85	942116	0	0	0.270	–

TABLE VII

RESULTS OF NUMERICAL COMPUTATIONS
FOR $\Delta x = 0.046296$ AND $L/h_o = 10.0$

θ°	N_S	N_{RS}	N_R	S(θ)	R(θ)
5	0	0	20712	1.000	1.000
10	0	0	11522	1.000	1.000
15	0	0	4244	1.000	1.000
20	0	0	962	1.000	1.000
25	0	0	96	1.000	1.000
30	0	0	8	1.000	1.000
35	0	0	0	1.000	–
40	0	0	0	1.000	–
45	0	0	0	1.000	–
50	0	0	0	1.000	–
55	0	0	0	1.000	–
60	0	0	0	1.000	–
65	638	0	0	0.999	–
70	7392	0	0	0.991	–
75	41806	0	0	0.954	–
80	153710	0	0	0.830	–
85	404521	0	0	0.552	–

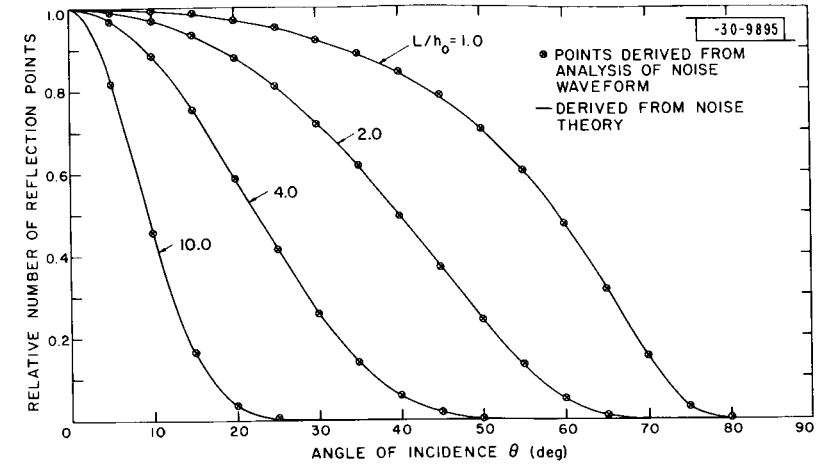

Fig. 18. Relative number of reflection points plotted against angle of incidence as obtained from noise theory and from computer program.

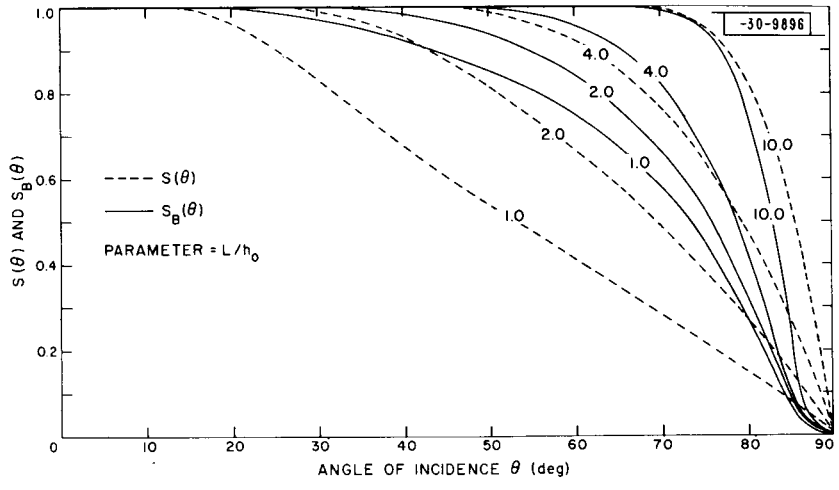

Fig. 19. Comparison of shadowing functions S(θ) and $S_B(\theta)$.

The relationship between N_R and Θ can be determined directly from noise theory (Kac, 1943). It is known that for a zero mean gaussian variable f with variance ψ_o the probability of f passing through a level F is proportional to:

$$P(F) \sim \exp[-F^2/2\psi_o] \quad . \tag{26}$$

In our example the slope df/dx is a zero mean random variable with variance

$$\left\langle \left(\frac{df}{dx}\right)^2 \right\rangle_{avg} = -h_o^2 \left.\frac{d^2\rho}{d\delta x^2}\right|_{\delta x=0} = 2h_o^2/L^2 \quad . \tag{27}$$

Hence, the probability of the perpendicularity condition being fulfilled for $df/dx = \tan\Theta$ should be:

$$P(\tan\Theta) \sim \exp[-L^2 \tan^2\Theta/4h_o^2] \quad . \tag{28}$$

This function is shown fully drawn in Fig. 18. The values determined by analyzing the noise waveform for specular points are shown on the same plot and for the same parameters. The agreement between the direct analysis of the noise waveform and the predictions from noise theory is seen to be exceedingly good.

As a further check on the results we compare the derived function $S(\Theta)$ as defined in Eq. (9) with the expression for this function given by Beckmann (1965a) for the fraction of the surface in the shadow, viz:

$$S_B(\Theta) = \exp[-\tfrac{1}{4}\tan\Theta \operatorname{erfc}(L/2h_o \cdot \tan\Theta)] \quad . \tag{29}$$

for the same values of L/h_o for which we carried out the analysis of the noise waveform. As can be seen from Fig. 19 where both $S(\Theta)$ and $S_B(\Theta)$ are plotted for comparison, the two functions can at best be said to be in qualitative agreement in that they approach unity at $\Theta = 0$ and zero at $\Theta = 90°$. That is, the expression given by Beckmann (1965a), i.e., Eq. (29) does not agree with our numerical analysis even when we assume Beckmann's definition [Eq. (9)] for the role played by shadowing is correct. The violent and unexpected discrepancy between the two functions led us to suspect that section of our program which evaluates the fractional part of the surface which is in the shadow. In order to put this section of the program to a test we replaced the sequence of correlated noise samples by a sequence of samples taken on a sinusoidal waveform. For this type of waveform it is possible to estimate the fractional part of the surface which is in the shadow as a function of angle of incidence as follows. The point x_1 where the surface enters into the shadow is determined by:

$$\frac{df}{dx} = \frac{d}{dx}(a \sin\alpha x) = a\alpha \cos\alpha x = -\operatorname{cotan}\Theta \tag{30}$$

and

$$x_1 = \arccos(-\operatorname{cotan}\Theta/a\alpha) \quad . \tag{31}$$

The point x_2 where the surface emerges from the shadow is determined from the equation

$$a \cdot \sin \alpha x_1 \, (x - x_1) \operatorname{cotan} \Theta = a \sin \alpha x \tag{32}$$

The shadowing function $S(\Theta)$ therefore becomes

$$S(\Theta) = \frac{x_2(\Theta) - x_1(\Theta)}{2\pi} \quad . \tag{33}$$

Figure 20 compares the results obtained from (33) with the results obtained from the computer program applied to sinusoidally varying samples – approximately 101 samples per cycle. The actual sinewave used in the comparison was of the form:

$$f(x) = 0.183 \cdot \sin (x \cdot 13.45) \quad . \tag{34}$$

The noise samples were picked from the formula:

$$f_i = 0.183 \cdot \sin (0.0623 \cdot i) \tag{35}$$

and $\Delta x = 0.00463$. The comparison shows that there is very good agreement between the results obtained by the two methods. We are therefore forced to the conclusion that the function $S(\Theta)$ found from the analysis of the noise samples is the correct shadowing function in Beckmann's sense in the particular case under consideration. We are, furthermore, led to believe that the expression given by Beckmann [Eq. (29)] is either misinterpreted by us or is incorrect.

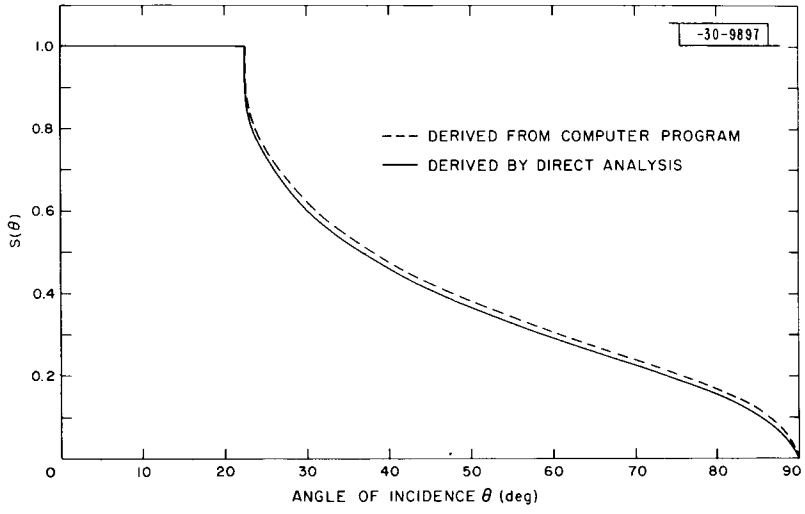

Fig. 20. Test of computer program for sinusoidally varying surface.

The discrepancy between $S(\Theta)$ that Beckmann (1965a) should have arrived at, and $S_B(\Theta)$ that he actually reached, possibly due to mathematical errors, makes it difficult to prove the point made in the introduction. If we take $S(\Theta)$ as representative of the correct shadowing theory, then an examination of Tables IV and V clearly indicates that the simple shadowing theory overestimates the effect of shadowing with respect to the theory which considers the fraction of reflection points which are in the shadow represented by $R(\Theta)$ as purported in the introduction. When $L/h_o = 4.0$ and 10.0 as in Tables VI and VII a comparison between $S(\Theta)$ and $R(\Theta)$ is no longer possible because of the extremely small number of reflection points obtained at angles Θ

large enough for shadowing to be of importance. If, on the other hand, $R(\Theta)$ is compared with Eq. (29) (which we do not believe to be the correct shadowing function on the basis of Beckmann's premises) it turns out that $S_B(\Theta)$ appears to underestimate shadowing when $L/h_o = 1.0$ and overestimate it when $L/h_o = 2.0$.

Beckmann (1965a) may have arrived at an erroneous expression [Eq. (29)] for $S(\Theta)$ as a result of mathematical error as pointed out by Shaw (1966).

We are, therefore, forced to conclude in general that recently advanced theories which attempt to explain the scattering from the lunar surface in terms of Kirckhoff theory and with shadowing included are erroneous and tend to overestimate the effect of shadowing. The excellent agreement obtained between theory and experimental results, we think, is fortuitous and certainly cannot be claimed as a proof that Kirckhoff theory with locally plane boundary conditions can be validly applied to lunar returns for all angles of incidence. We are still of the opinion that the return at oblique angles of incidence must be explained in terms of discrete small scale scatterers having a radius of curvature comparable with the wavelength of the exploring wave and thus violating the basic assumptions made in Kirckhoff theory.

II. PLANS AND PREPARATIONS

At the commencement of the contract period the Lincoln Laboratory Millstone Hill Radar was ready for use for lunar radar studies. As indicated in QPR (1966:1) 23-cm measurements have, therefore, been able to go forward without delay. The Haystack 3.8-cm radar was not operable for lunar studies during the first four months of the contract, and only became so during this reporting period. However, there remain restrictions upon what can be accomplished with this instrument at the present time. In particular it is not presently possible to employ the radar to make fine resolution radar maps of the moon's reflectivity. The work which must be performed before this can be accomplished is outlined in Sec. II-A below. As can be seen, this additional capability will be brought about by the completion of a number of computer programs (outlined in Sec. II-A-1) and the construction of some additional items of equipment (Sec. II-A-2). Work in all these areas has commenced but may not be completed for a further 2 to 3 months.

In order to gain some operating experience, and test those parts of the equipment and the computer programs that are complete (or nearly so), we intend to continue to operate the Haystack radar in conjunction with the Millstone data recording facilities. Instrumental limitations in these recording facilities (which are inferior to those being provided but not yet completed for Haystack) preclude the possibility of making maps containing the full resolution that is both possible and planned. Accordingly, this interim arrangement will serve mainly to establish the overall procedure to be employed later when the work of readying Haystack is complete. The interim scheme can be put into effect with the addition of only one computer program for the Millstone SDS 9300 computer, which will perform the function of transcribing data samples into a magnetic tape record having the proper format.

Whereas the Haystack radar has begun some of its program of observations and should be ready to embark on the mapping program some time this summer, the Lincoln Laboratory 8-mm radar requires a considerable amount of engineering design development and construction before it will be ready. The nature of the work is outlined briefly in Sec. II-B.

A. PREPARATIONS FOR 3.8-cm MAPPING

1. Computer Program Development

The computer programs required for the Haystack CDC 3200 to provide radar maps of the lunar surface fall into four main categories:

(a) Pre-run calculations and planning
(b) Real-time tracking of a point on the lunar surface
(c) Real-time data processing of radar returns
(d) Post-run mapping of data onto lunar surface.

The programs that will accomplish these tasks are outlined in this report and a block diagram of their relationship is shown in Fig. 21.

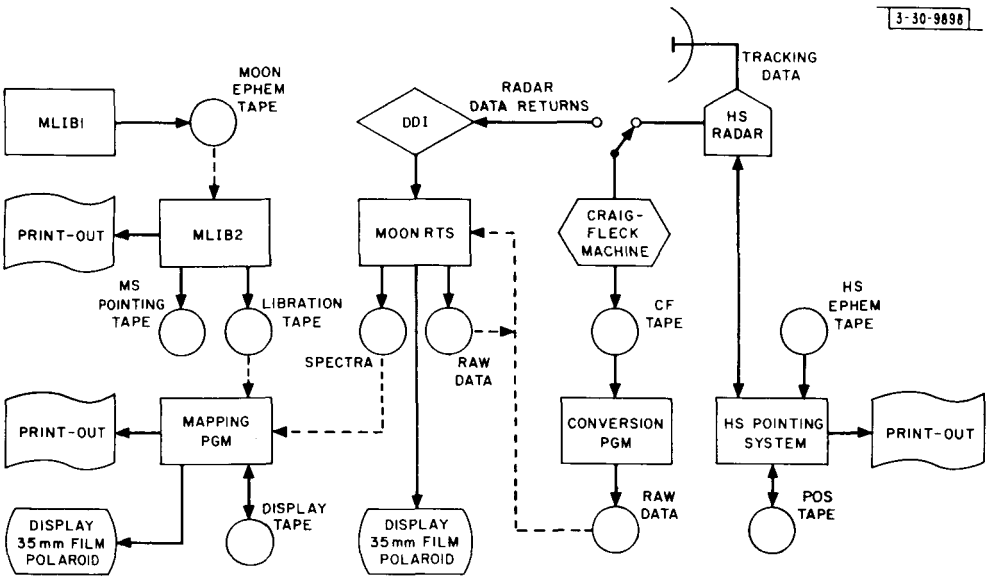

Fig. 21. Block diagram of computer programs required for lunar mapping at 3.8 cm.

a. Pre-run Calculations

The Moon Libration Program, MLIB, performs all non-real time calculations required for lunar work at Millstone and Haystack. The basic output of this program is a printout of azimuth, elevation, range, Doppler, and related quantities for the sub-radar point. Four options are available.

(1) Millstone Mode – Provides basic output, setting for Millstone range tracker, and a pointing tape.

(2) Offset Mode – Provides basic output and similar printouts for specified points on the lunar surface.

(3) Haystack Mode – Provides basic output and a libration tape for input to the mapping program (see Sec. II-A-1-d).

(4) Planning Mode – Provides printout of observation periods for standard LAC quadrants, including resolution statistics.

MLIB can be run for any ground station. It requires a binary moon ephemeris tape as input. This tape is prepared from Naval Observatory data (most of which is supplied to us on punched cards) once each year.

b. Real-Time Tracking

The Haystack antenna is pointed by digital commands from a Univac 490 computer. The original pointing programs provided for real-time tracking of the lunar sub-radar point only. An addition has been made to allow for tracking in azimuth, elevation, range, and Doppler of a specified point on the lunar surface. The point may be designated in four ways:

(1) Selenographic latitude and longitude

(2) Direction cosines in selenographic coordinate system

(3) Direction cosines in observer coordinate system

(4) Delay and angle.

c. Real-time Data Processing

A real-time data processing program, MOONRTS, has been written for the CDC 3200. This program will accept the raw radar data, record it on magnetic tape, reformat and edit the data, and compute the echo power spectrum for each range interval over a specified integration period. The spectra are then recorded on magnetic tape for input to the mapping program (see Sec. II-A-1-d).

There are three modes of inputting the radar data:

(1) NORMAL: Data are stored directly into the CDC 3200 computer core via the Direct Data Interface (DDI).

(2) TAPE: The raw data tape, recorded on a previous run, replaces the DDI. This allows us to "replay" a run if desired.

(3) SIMULATION: In this mode a signal of known frequencies is generated by the program, formatted to look like raw data from the DDI and stored on the disk file for input.

The program utilizes a Tukey-Cooley subroutine to perform the Fourier analysis and a package of disk file routines for data storage and retrieval. A planned display portion remains to be implemented. This will allow simple monitoring of the data reduction process in real time.

Because of the unavailability of certain hardware at Haystack, the first cut at actual data processing will use the range-tracking machine at Millstone. Haystack radar data will be sampled and digitally recorded on magnetic tape. A program is being written to convert the tape recorded at Millstone to the same format as the raw data tape created by MOONRTS. This tape will then become input under the existing TAPE Mode.

d. Post-Run Mapping

The mapping program uses tapes from MLIB and MOONRTS as input. The latter tape provides power vs frequency for each range gate as a function of time. Certain range gates represent samples of noise and others of noise plus a calibration pulse. These will be used in normalizing the signal plus noise data. The purpose of this program is to transform the power from the radar coordinate system involving delay and frequency to a coordinate system of selenographic latitude and longitude. The data from consecutive coherent integration periods are incoherently integrated until the mutually sliding coordinate systems demand a new transformation. The MLIB tape provides the information necessary to determine these intervals. The data are corrected for the effect of the beam pattern and scattering law, and are normalized to remove variations of the radar parameters. Final output will consist of a data file either on a disk or on tape which will be the input to a display routine. There the maps will be displayed on a monitor scope and/or photographed.

The program, as presently planned, does not include calibration or display capability.

In conclusion, some portions of the lunar mapping software system are entering the test stage, but considerable programming effort remains. Appropriate contract help is being sought.

2. Equipment Development

As mentioned earlier, a short pulse ranging capability became available in the Haystack system during this quarter. The lunar pulse measurements outlined in Sec. I-B-2 were possible only by making use of the Millstone Hill data processing and timing equipment and the intersite coupling. It is not feasible to do the full lunar studies measurements task in this way. There remains some vital construction to be accomplished at Haystack, particularly in the data processing and timing areas, before fully self-contained operations can be undertaken. The status of various important components is as follows:

(a) The transmitter is operational. It must, however, still be used at slightly reduced power (75 kw) because of limitations in the series-beam switch regulator.

(b) The analog-to-digital converter and multiplexer system to be used to introduce signal data into the CDC 3200 real-time data processing computer is virtually complete. The computer interface has been checked out. There remains only the connecting of real-time clock data to the computer and the interfacing of the radar timing system to the analog-to-digital converter controls.

(c) A low frequency amplifier, filter, and phase detector system is currently under development. This sub-system accepts 2-Mcps data from the radar receiver and converts it to a zero frequency signal (through phase detectors), producing quadrature components of the signal. These video signals are then passed through matched filters and converted to digital data for processing by the computer.

(d) The radar receivers are operational. Work is currently in progress to provide an improved signal calibration system and easier conversion between various experimental arrangements such as changing from linear to circular polarization. The receivers have been operated without the benefit of cooled parametric amplifiers for lunar work during this quarter. With cryogenic cooling, a system temperature of 200°K is possible.

(e) Radar system timing required for the lunar mapping is the largest piece of equipment remaining to be constructed. The timing equipment must control the transmitter modulation and receiver TR gating. It also must control the analog-to-digital converter and reference calibration timing with an offset rate so that the motion of the moon is tracked automatically in range.

(f) The equipment required to control the receiver Doppler frequency timing from the U490 pointing computer is complete but has not been checked.

B. PREPARATIONS FOR 8-mm OBSERVATIONS

A 28-foot parabolic antenna system operating at the shortest wavelength (8.6 mm) that we plan to employ for lunar studies, is mounted on the roof of the main Laboratory building. Despite being the smallest of the three antennas, the 28-foot parabola has the highest gain by virtue of its short operating wavelength. This parabola was formed by a spincasting process in which a $\frac{3}{8}$-inch layer of polymer was made to take up the proper parabolic shape by spinning the metal and fiberglas support structure. A thin reflecting layer of zinc was flame-sprayed over the polymer and this in turn was given a thin coating of plastic to protect it from the weather. This method of constructing large precision parabolas has been described by Dawson (1962).

In order to feed an antenna of this size at millimeter wavelengths a special "rear feed" was devised. This consists of an open-ended circular waveguide operating in its dominant mode

(TE_{11}) with a circular reflecting disk positioned approximately 3.5 wavelengths in front of the open guide. A small hemispherical radome serves to hold the reflecting disk in position and also provides weather protection. The system may be likened to a Cassegrain feed arrangement in which the feed point has been chosen so close to the prime focus that a plane secondary reflector is required in place of the hyperbolic subreflector normally encountered. This novel feed arrangement has an advantage over most other types in that no large supporting struts are required, which would introduce aperture blockage and increase the sidelobe levels. The feed design has been described by Keeping (1960) and the electrical performance of the antenna has been reported by Fitzgerald, et al. (1963).

The antenna was installed on the roof of one of the main Laboratory buildings in Lexington in 1962, and employed to make radar studies of the moon in April and May 1963. The performance of the antenna can rapidly be checked at any time using permanently installed pattern measurement equipment. To permit focusing of the antenna without the use of flexible waveguide or movable joints, all the microwave components of the radar and pattern receiver are mounted on a single large plate in the equipment housing. Adjustment is accomplished by movement of the entire plate and feed. Horizontal polarization is employed. The antenna is mounted on an azimuth-elevation drive system, which, unfortunately, is inadequate to permit the use of position-servo drives. The prime method of directing the beam is manual control of rate-feedback-servo loops with reference to a boresighted-television system. To avoid errors due to inaccurate gearing and flexibility of the mount base, the 6-inch lens system and television camera are installed directly on the reflector backup structure. The rate-servo controls and television monitor are located in a nearby building along with the other non-microwave portions of the multiplier.

The 10-watt transmitter consisted basically of a floating-drift-tube klystron oscillator phase-locked to the required frequency which was generated by a crystal-controlled frequency-multiplier chain. The spectral width of the radiated signal was not more than 100 cps. The receiver was a multiple superheterodyne which converted the incoming signals to a nominal IF of 2.5 kcps where it was examined in a bank of ten filters 170 cps wide and spaced 100 cps apart. A filter bank at the output was used because of uncertainty as to the stability of the multipliers; it also guarded against signal loss in case of incorrect Doppler compensation. The first stage in the receiver was a crystal mixer. Further details of this radar system have been given by Lynn, et al. (1963).

Since its use as a moon radar in 1963, the 28-foot parabola has been employed largely for radiometric observations at 1.5-cm wavelength. For this purpose a larger feed line has been installed which may, if used at 8 mm, yield a 2-db improvement in the performance of the radar. However, it is possible that when coupled to the diameter-reducing taper (required to illuminate the dish properly at 8-mm wavelength) this large feed line may develop high loss due to the trapping of unwanted modes. A set of experiments using the antenna range has so far failed to reveal any evidence of high loss. Further tests on the loss in the line with taper will be made on the bench. These tests require special waveguide connections which will take two months to procure.

As a first step in reactivating the radar it is proposed to reinstall the 10-w equipment employed by Lynn, et al. (1963). Some components of this system have been rebuilt. These

modifications have provided an improvement in the overall frequency stability (now 5 cps) and the reliability. The transmitter power will still, however, be only 10 w, which is quite inadequate for the work planned. Lunar reflection measurements made with this radar will serve to familiarize the engineers with the equipment and operating procedure, but are unlikely to add significantly to the results reported by Lynn, et al. (1963).

A higher power transmitter is of the utmost importance. A modest increase (to 50 w) is expected in June when two 50-w tubes (originally scheduled for delivery on 15 February) should arrive. It is not clear at present whether it will be more difficult to phase-lock these tubes than the existing 10-w tube.

For measurements in which any degree of detailed resolution (either in delay or frequency) is required, a much larger increase in transmitter power is vital. Negotiations have been conducted for the construction of a 1-kw tube, and a purchase order will be placed. Delays in approvals for the procurement of the 1-kw tube seem likely to delay the start of the lunar observations with the high power transmitter. Also required for the high power transmitter is a new frequency multiplier chain having a higher level output and better frequency stability than the existing one. There has been considerable difficulty in getting bids on this multiplier chain and also in getting a source (at 5 Mcps) with a spectrum pure enough to withstand multiplication to 35 Gcps. These troubles now appear to have been overcome; orders have been placed for oscillators and multiplier chains that promise to be satisfactory.

Extensive investigations have been made of the possibility of obtaining a two-channel parametric amplifier that would yield an appreciable increase in sensitivity. There seems little prospect that this can be accomplished in the time available, and for the duration of the present program balanced mixers will be employed as first stages in the receivers.

The high-power radar will have the capability of (1) transmitting circular polarization and receiving circular polarization in the same sense and in the opposite sense; (2) transmitting circular and receiving two orthogonal linear polarizations, oriented at will; (3) transmitting linear polarization, oriented at will, and receiving that linear polarization and the orthogonal one. Waveguide elements for performing these functions have been designed, and the mandrels for electroforming them are now being made.

Operation at low power (either 10 or 50 w) is expected this summer. Full high power operation is hoped for during the first quarter of 1967.

III. NOTES ON FUTURE WORK

A. EXPERIMENTS TO DETERMINE THE DEPTH OF A LUNAR SURFACE LAYER

1. Introduction

The purpose of this section is to consider how it might be possible to determine the depth of the upper layer of light material on the lunar surface by radio methods. One of the most direct approaches to placing some limit to the depth would be to repeat the experiment performed by Hagfors, et al., as described in QPR (1966:1), at increasing wavelengths. Thus, in the next section we discuss the way the experiment could be conducted at longer wavelengths where difficulties will be encountered due to ionospheric effects. In Sec. III-A-3 we discuss another approach which depends for success on the layer being of roughly constant thickness over moderately large regions of the lunar surface. The experiment would, however, reveal the presence of a continuous gradation in density with depth (should this be the case). These schemes are probably unsuitable for determining the layer depth if this is substantially greater than 4 to 5 m. If the depth is very great (e.g., 100 m), then it appears that it could be determined, at least in principle, from short pulse experiments that are discussed in Sec. III-A-5.

2. Polarization Experiments at Longer Wavelengths

The depth of the layer of light material is presumed to be irregular but must be greater than about one wavelength for pronounced polarization effects to be observed. A straightforward way to attempt to place an upper limit on the depth of the layer would be to repeat the experiment described in Sec. I-J of QPR (1966:1) at increasing wavelengths, until the polarization effects disappear. Unfortunately this is more difficult than is at first obvious for the following reasons.

(a) Ionospheric Faraday rotation of a linearly polarized wave increases with wavelength as λ^2. At a wavelength of 23 cm the Faraday rotation of a plane wave in the earth's ionosphere is usually not larger than about 10° and hence can be compensated or even neglected. For a wavelength of 3 m the one way Faraday rotation may be as large as 10 or so complete rotations. Variations occur over short periods of time due to both the changing geometry of the ray path through the ionosphere (as the moon's motion is followed), and the diurnal variations of the electron density in the ionosphere. At midlatitudes the rate at which the total rotation may change has been found on occasion to be as high as 4°/minute at a wavelength of 3 m.

(b) In the observations performed at Millstone Hill an adequate resolution in the frequency domain could be obtained using 2-cps filters. However, the overall bandwidth of the reflected signals varies as $1/\lambda$ and thus to obtain the same resolution at 3 m one would require filters ~ 0.16 cps wide.

Faraday rotation may be expected to be sufficiently serious at all wavelengths longer than about 30 cm so that it could not be ignored. In order to remove the effects of Faraday rotation it would be necessary in fact to determine continuously the total amount of rotation Ω. This could be accomplished by transmitting a linearly polarized wave (in place of a circular one) and receiving both orthogonal components.

By comparing the intensity of the two components one would obtain the ambiguous fractional rotation $\Delta\Omega$ where

$$\Omega = n\pi \pm \Delta\Omega \pm \pi/2 \quad . \tag{36}$$

However, by repeating the observations at another frequency separated from the first by df, Ω can be determined from the observed change $d\Omega$ from

$$\frac{d\Omega}{\Omega} = 2f \cdot df \tag{37}$$

where f is the radar frequency. In practice one might transmit alternate pulses at the two frequencies and hence continuously determine $d\Omega$. From these measurements it would be possible later to determine Ω as a function of time. One could then select from the observations those periods where the transmitted linear signal lay parallel to or perpendicular to the axis of the moon's libration. By processing these periods to obtain the echo power as a function of delay for the center Doppler strip only, one would be able to obtain the ratio of the two transmission coefficients.

Whereas in principle it should always be possible to compensate for Faraday rotation (effect a), it will not always be possible to maintain the frequency resolution of the radar necessary to resolve a central strip of the disk as the wavelength is increased (effect b). We have seen that for $\lambda = 3$ m we require a filter width of the order 0.16 cps. This might be comparable with or less than the frequency stability imposed by phase fluctuations in the ionosphere. The filter width that can be achieved ultimately depends upon (a) the overall stability of the radar system (which probably improves with increasing wavelength), and (b) the stability of the propagation medium.

The Millstone Hill radar operating at 23 cm has been shown to have an overall frequency stability, i.e., (a), above, on the order of 0.1 cps (Evans, et al., 1965), and it is expected that at longer wavelengths even better stability should be realized, since fewer multiplications of the basic frequency standard are required. It seems safe to assume that an overall stability of better than 0.05 cps should be obtainable at 3-m wavelength.

The influence of the ionosphere on the frequency stability of radar transmissions, i.e., (a), above, has not been the subject of much experimental investigation. Irregular density fluctuations are known to be present for much of the time and these give rise to scintillations of radio stars. The density fluctuations may be seen on ionospheric sounders as Spread F echoes. The world-wide occurrence of Spread F is shown in Fig. 22. For the northern hemisphere the occurrence rate is least between 30° and 50° geomagnetic latitudes. Observations of the moon at 7.84-m wavelength have been conducted from within this range of latitudes (Evans and Ingalls, 1962) and the echoes were found to be spread by ionospheric scintillations according to

$$P(f)\, df \propto \exp\left[-\frac{1}{2}\left(\frac{\Delta f}{\Delta f_m}\right)^2\right] df \tag{38}$$

where P(f) is the power spectrum of the fluctuations and Δf_m had a value of 0.2 cps. It is anticipated that the mean intensity of these fluctuations varies as the secant of the zenith angle

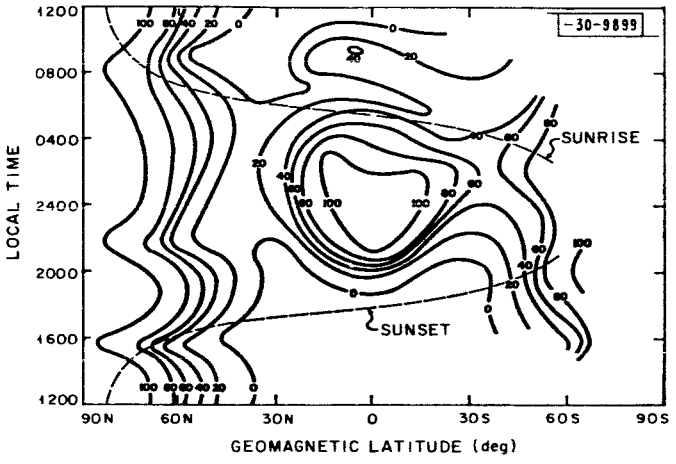

Fig. 22. Percentage occurrence of Spread F as observed by the topside sounder Alouette. Spread F is associated with ionospheric scintillations of radio sources.

and inversely as the square of the wavelength. In the most favorable circumstances, when observations are conducted with the moon in the zenith at say 30°N geomagnetic latitude, we might anticipate that the spectral broadening introduced by the moon and the ionosphere will on the average be roughly comparable at a wavelength of about 6 m. On occasion the effective "seeing" may be considerably better but this would not be known a priori.

In conclusion then, it is considered that the Millstone Hill experiment could be repeated without serious difficulty at wavelengths up to 3 m, and under favorable circumstances perhaps to 6 m, but not at longer wavelengths due to the phase instability imposed by the ionosphere.

3. Other Observations

A second type of measurement which would yield the depth of the layer of light material is based upon observing interference effects. Let us suppose that a small area on the lunar surface may be isolated in which the layer depth d is comparatively uniform. At normal incidence the reflection coefficient will be

$$R(0) = \frac{R_1 + R_2 + 2\sqrt{R_1 R_2}\,(1 - 2\sin^2 2\pi d/\lambda}{1 + R_1 R_2 + 2\sqrt{R_1 R_2}\,(1 - 2\sin^2 2\pi d/\lambda} \qquad (39)$$

where R_1 is the reflection coefficient of the upper interface and R_2 that of the second interface. It can be seen that the reflection coefficient is greatest for $d = \lambda/2,\ \lambda,\ 3\lambda/2$ and least for $d = \lambda/4,\ 3\lambda/4,\ 5\lambda/4$. When d has a value of $m\lambda/4$ the reflection coefficient may fall to a very low value if $R_1 \approx R_2$ corresponding to $\epsilon_1 \approx \sqrt{\epsilon_2}$. In practice the variation of the depth d over the surface will cause the reflection coefficient to change less with wavelength than predicted by (39). If the actual depth departs from the mean in a random fashion we may expect the depth of the first minimum in the reflection coefficient to be decreased. Successive minima corresponding to $d = 3\lambda/4,\ 5\lambda/4$ will be more seriously affected and may be totally obscured. It may be therefore, that only the first minimum can be recognized. Table VIII gives the operating frequencies

TABLE VIII

FREQUENCIES AT WHICH THERE WILL BE A MINIMUM IN THE REFLECTION COEFFICIENT FOR DIFFERENT VALUES OF THE LAYER THICKNESS d

Minimum	Frequency (Mcps)		
	d = 1m	d = 5m	d = 25m
$\lambda/4$	75	15	3
$3\lambda/4$	225	45	9
$5\lambda/4$	375	75	15
$7\lambda/4$	525	105	21
$9\lambda/4$	675	135	27

at which minima might be expected for values of d = 1, 5 and 25 meters. It can be seen that the minima are evenly spaced in frequency, and because reliable measurements cannot be made from the earth at frequencies of less than about 20 Mcps (owing to ionospheric effects) the first minimum may not be observable if d > 5 meters.

Let us suppose that a search is to be conducted for a minimum in the radar cross section using the 1000-ft antenna at the Arecibo Ionospheric Observatory. In order to isolate a region in which the waves are near-normally incident on the lunar surface, a pulse length of 100 μsec might be employed, and the echo from the leading edge only examined. Such a pulse would illuminate a region at the center of the visible disc having a radius of about one tenth the lunar radius. Thus the range of values of angles of incidence encountered would be from 0 to 7°. Table IX lists the assumptions made in the calculations in order to arrive at a list of the parameters of the radar system that might be required. These parameters are then listed in Table X. It has been assumed that a signal-to-noise ratio of 10 db is required, and that a receiver bandwidth of 10 kcps is employed in order to match the spectral width of the transmitter pulse. The system temperatures assumed are those of the sky background in directions away from the plane of the galaxy or the sun. The increase in temperature with wavelength, together with the reduced antenna gain, are jointly responsible for the higher transmitter powers required at the longer wavelengths. If an antenna the size of the Jodrell Bank Mk I i.e., 250-ft diameter, were to be employed, the transmitter powers required would be some 250 times those listed in Table X.

Ionospheric scintillations should not hamper an experiment of this kind as we require phase stability only over an interval equal to the length of the tramsmitter pulse (100 μsec). However, Faraday rotation would need to be compensated either by transmitting and receiving circularly polarized waves or by transmitting one linear and receiving both orthogonal components.

Several difficulties exist in an experiment of this type which should be touched upon. Due to the libration of the moon, the subradar point will be different from day-to-day, and consequently the value of d may vary with the time of observation. It would, therefore, be preferable to make observations over the entire frequency range of interest in as short an interval of

TABLE IX

ASSUMPTIONS MADE IN COMPUTING THE TRANSMITTER POWER REQUIRED FOR LONG WAVE OBSERVATIONS OF THE MOON AT THE ARECIBO IONOSPHERIC OBSERVATORY

Total radar cross section	$0.07\pi a^2$
Fraction of total cross section observed using a 100-μsec pulse	40 percent
Pulse length	100 μsec
Receiver bandwidth	10 kcps
System temperature	Set by sky background (see Table IV)
Antenna employed	1000-ft spherical reflector at Arecibo, Puerto Rico
Antenna efficiency	40 percent
Required signal-to-noise ratio	+10 db

TABLE X

PARAMETERS OF LONG WAVE RADARS EMPLOYING THE 1000-FT ANTENNA AT ARECIBO

λ (m)	f (Mcps)	Antenna Gain (db over isotropic)	System Temperature (°K)	System Transmitter Power (w)	Observing Time (min)
3.3	100	46	$10^{3.0}$	1.5	70
5	60	42	$10^{3.5}$	13	120
7.5	40	39	$10^{4.0}$	90	210
10	30	36	$10^{4.3}$	300	240
15	20	32.5	$10^{4.7}$	2000	350
20	15	30	$10^{5.0}$	5000	480

time as possible. Radio echoes from the moon fade, however, and an average over many fading cycles must be taken in order to reduce the uncertainty in the value for the mean echo power. For the leading edge echo observed at 100 Mcps the fading period would typically be 10 seconds, and will increase linearly with wavelength. Thus, if we are to reduce the resulting uncertainty in the measurements to say ±5 percent, we require the observing times listed in the last column of Table X. At 15 Mcps the time required (8 hours) is longer than the time for which the moon may be viewed from the Arecibo instrument in a single day. Even if a sacrifice in the accuracy is made, it is clear that a swept frequency radar system cannot be employed at the longest wavelengths. A separate radar system is required for each frequency that is to be examined. The problems of operating so many radar systems simultaneously are not insuperable, but clearly the experiment constitutes a major undertaking.

Let us suppose that a system has been devised which will measure the lunar radar cross section at intervals of say 5 Mcps over the range 15 to 100 Mcps. There remains the problem of accurately calibrating these radar systems. Ideally one would do this against a target of known cross section, for example, a metal sphere placed in earth orbit. A 1-m^2 sphere placed in a synchronous orbit would be a poorer target than the moon by 100 db. It follows that the sphere must be placed in a lower altitude orbit. Further, the sphere must have a large diameter (e.g., 5 m) so that its cross section will remain appreciable when observed at the longest wavelength. An altitude of about 1000 to 2000 km might be adequate, but unfortunately it would no longer be possible to calibrate the radar systems at will – e.g., during the course of the measurements. The alternative to using some form of test target is to determine separately the radar parameters of each of the systems. The transmitter powers and system temperatures can usually be determined adequately, but there is no simple method by which the antenna gains could be established in the case of the Arecibo antenna, where the gain is a function of the zenith angle.

Many of the problems encountered in this experiment (in particular the ionospheric effects) could be obviated by placing the radar(s) in a satellite in orbit about the moon. However, a new set of problems then arises owing to the motion of the satellite causing it to sample different areas of the surface beneath.

4. Other Models of the Surface

Giraud (1965) has considered a model of the surface in which the dielectric constant ϵ increases from unity linearly with depth over some finite distance d and then becomes constant at some value ϵ_2. Figure 23 shows the variation of reflection coefficient to be expected for the case $\epsilon_2 = 5$ for a number of values of d. The same type of experiment described in the previous section would provide a test of this model. Because one would not now be searching for a minimum k in the reflection coefficient but simply a wavelength dependence, a wider spacing of the frequencies might be employed. The reflection coefficient reaches that attributable to the base layer alone when the wavelength $\lambda \approx 30\,d$. Since the observations would be limited to wavelengths $\lambda \leqslant 20$ m by ionospheric effects, the full range of reflection coefficients will not be encountered if the layer depth d exceeds about 1 meter. The fact that this model may be correct would not then be recognized. Here a satellite experiment, i.e., a lunar orbiting vehicle, may provide the

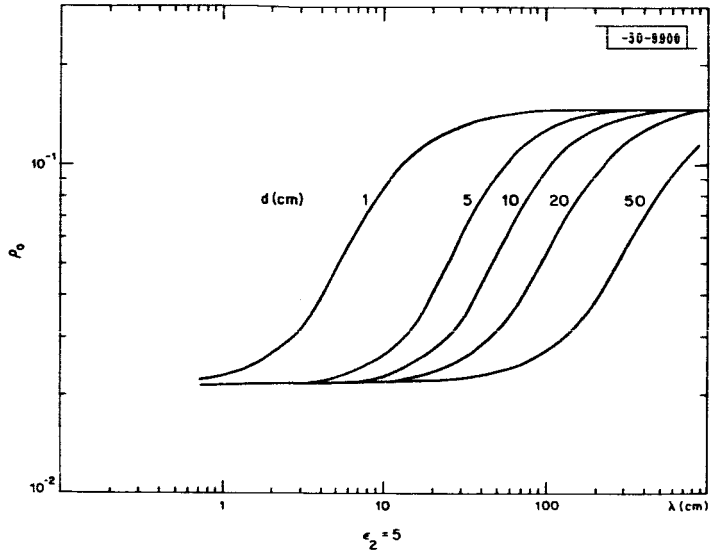

Fig. 23. Variation of reflection coefficient of surface in which uppermost layer has a dielectric constant that increases linearly with depth over a distance d and then becomes constant at $\epsilon = 5.0$.

solution, but an accurate calibration of the multifrequency radar system employed would be extremely difficult.

5. A Very Deep Layer

None of the methods discussed so far would be capable of determining from earth the depth of a very deep layer of material, i.e., $d > 5$ m. The most direct method to be employed in such a case would be to use an extremely short pulse radar and search for echoes separated in delay arising from reflections at each interface. In order to remove the dispersion of the echo due to the variation of surface height it would be desirable to localize a region at the center of the lunar disc using extremely high angular resolution afforded by a large antenna. The curvature of the moon's surface will cause the mean height h to vary by an amount

$$\Delta h = \ell^2/a \tag{40}$$

where ℓ is the radius of the illuminated region and a the radius of the moon. Let us suppose that the depth of the layer d is 100 meters. Since we require that $d >> \Delta h$ let us take a value $\Delta h = 15$ m. The region illuminated would be required to have a radius $\ell = 4$ km. This could be isolated with an antenna having a diameter of 5×10^4 wavelengths. Unfortunately there are few antennas in existence having diameters as large as 10^3 wavelengths, and hence this scheme is impracticable at present.

The remaining possibility open to us is that of performing an aperture synthesis. In this experiment the autocorrelation function of the echoes from the center of the disc is obtained repeatedly throughout a day when the direction of the axis of libration changes by 180°. It is then possible to construct the two dimensional autocorrelation function of the complex echo

amplitude whose double Fourier transform is the brightness distribution. By performing this operation at successive range intervals we should encounter a point where the echo from the second interface lies in the center of the brightness plot, and that from the upper interface at the same range lies in a halo around it. In order to achieve an adequate range resolution to recognize a layer of 100 meters depth we would require a pulse length in the range 10 to 30 nanosec. The duration over which the autocorrelation functions are formed would define the size of the synthesized aperture and hence the resolved region on the lunar disc.

Because ionospheric scintillation effects vary as λ^2 and the coherence time of the reflections as λ, there is a large penalty (λ^3) in attempting this experiment at a long wavelength. A suggested system would be to employ the Haystack antenna system at a wavelength of 3.8 cm. The radar would be required to be completely coherent for a period of more than 10 seconds in order to resolve regions of the surface having a radius of 2 km. Table XI lists the parameters of the radar system required. The path loss assumed is somewhat uncertain since the distribution of echo power with delay has never been determined using pulses as short as this. However, by extrapolating from earlier measurements at this wavelength Safran (1964) has obtained a value for the cross section of the lunar surface at normal incidence of 0 db per square meter. It follows that a region some 2 km in radius will have a cross section of $\sim 2 \times 10^7$ m^2 and that the path loss will be ~300 db. The transmitter power required is rather large. A reduction could be achieved by degrading the depth resolution from 1.5 m (a value obtained by matching the pulse length to the depth of the curvature of a region 2 km in radius) to, say, ten times as much. This would hardly be a serious loss since it is unlikely that the surface anywhere will be smoother than ~ ±10 m over a region some 2 km in diameter. This would reduce the required transmitter power to 6 MW which might perhaps be achieved using a 0.5-MW CW transmitter together with a 12:1 pulse compression scheme.

TABLE XI

PARAMETERS OF A VERY SHORT PULSE RADAR USING THE HAYSTACK ANTENNA

Assumed path loss	300 db
Frequency	8000 Mcps
Antenna gain	66 db
Pulse length	10 nanosecs (corresponding to a resolution in depth of 1.5 m)
Receiver bandwidth	100 Mcps
System temperature	10^3 °K
Peak transmitter power required for unity signal-to-noise ratio	6×10^7 W

6. Conclusion

We have outlined in QPR(1966:1) the radar evidence for the existence of a layer of light material on the lunar surface, and here we considered several ways in which the depth of this material might be established. The first of these would simply be to repeat the experiment in which the presence of this material was recognized, at longer wavelengths. It seems that this procedure might be satisfactory for a depth of less than 3 meters. Due to the limited phase stability of the earth's ionosphere, problems would be encountered in making observations at longer wavelengths. This would make it difficult or impossible to isolate separate regions of the lunar surface by spectral analysis of the echoes. The second method discussed can be applied at wavelengths of up to about 15 meters as it depends only on observing the reflection coefficient vs frequency. This method is exceedingly difficult to implement, but could detect a discontinuity in the lunar surface density at a depth of up to 4 meters. This same technique would also reveal a continuous gradation of density over a depth of 1 meter or less.

If the depth of the material is very large, e.g., 100 m, then it seems it might be inferred from observations in which extremely short pulses ($\sim 10^{-8}$ seconds) are used, to resolve the reflections from the two boundaries. In order to isolate a small portion of the lunar surface at the center of the disc that is normal to the ray path, a scheme of aperture synthesis would be necessary. This might best be accomplished at short wavelengths where ionospheric effects are negligible and the coherence time required of the radar hopefully can be achieved.

ACKNOWLEDGMENTS

The work of most of the technical personnel of Group 31, Surveillance Techniques, which operates the facilities of the Field Station, in preparing and conducting the work reported to date is gratefully acknowledged, as is the work of members of Group 46, Microwave Components, in cooperating with Dr. McCue on the 8.6-mm radar.

The use of the facilities of the Lincoln Laboratory Millstone-Haystack complex, provided by the U.S. Air Force, is also gratefully acknowledged.

REFERENCES

Beckmann, P., "Shadowing of Random Rough Surfaces," IEEE Trans. AP 13, 384-388 (1965a).

_____, "Radar Backscattering from the Surface of the Moon," J. Geophys. Res. 70, 2345-2350 (1965b).

Brunschwig, M., et al. (10 authors), "Estimation of the Physical Constants of the Lunar Surface," The University of Michigan Rep. 3544-1-F (1960).

Daniels, F.B., "Radar Determination of the Root Mean Square Slope of the Lunar Surface," J. Geophys. Res. 68, 449-453 (1963a).

_____, "Radar Determination of Lunar Slopes: Correction for the Diffuse Component," J. Geophys. Res. 68, 2864-2865 (1963b).

Davies, R.D., and Gardner, F.F., "Linear Polarization of Lunar Emission," J. Res. Natl. Bur. Standards 69D, 1613 (1965).

Davies, J.R., and Rohlfs, D.C., "Lunar Radio-Reflection Properties at Decameter Wavelengths," J. Geophys. Res. 69, 3257-3262 (1964).

Dawson, J.W., "28 ft. Liquid-Spun Radio Reflector for Millimeter Wavelengths," Proc. IRE 50, 1541 (1962).

Evans, J.V., Brockelman, R.A., Henry, J.C., Hyde, G.M., Kraft, L.G., Reid, W.A., and Smith, W.W., "Radio Echo Observations of Venus and Mercury at 23 cm Wavelength," Astron. J. 70, 486-501 (1965).

Evans, J.V., and Hagfors, T., "On the Interpretation of Radar Reflections from the Moon," Icarus 3, 151-160 (1964).

Evans, J.V., and Ingalls, R.P., "Radio Echo Studies of the Moon at 7.84-meter Wavelength," Technical Report 288, Lincoln Laboratory, M.I.T. (1962), DDC 204008.

Evans, J.V., and Pettengill, G.H., "The Scattering Properties of the Lunar Surface at Radio Wavelengths," The Moon, Meteorites and Comets – The Solar System, Vol. 4 (ed. Kuiper, G.P., and Middlehurst, B.M., Chapter 5, Univ. of Chicago Press, Chicago (1963a).

_____, "The Scattering Behavior of the Moon at Wavelengths of 3.6, 68 and 784 Centimeters," J. Geophys. Res. 68, 423-447 (1963b).

_____, "The Radar Cross-Section of the Moon," J. Geophys. Res. 68, 5098-5099 (1963c).

Fitzgerald, W.D., Lynn, V.L., and Keeping, K.J., "Experimental Evaluation of a 1000 Wavelength Antenna," Group Report 46G-4, Lincoln Laboratory, M.I.T. (1963), DDC 406109.

Gautschi, W., "Error Function and Fresnel Integrals," Table 7.2, Handbook of Mathematical Functions, ed. Abramowitz, M., and Stegun, I.A., Natl. Bur. Standards (1965).

Giraud, A., "Note on the Radio Reflectivity of the Lunar Surface," J. Res. Natl. Bur. Standards 69D, 1677-1681 (1965).

Grieg, D.C., Metzger, S., and Waer, R., "Considerations of Moon-Relay Communication," Proc. IRE 36, 652-663 (1948).

Hagfors, T., "Backscattering from an Undulating Surface with Applications to Radar Returns from the Moon," J. Geophys. Res. 69, 3779-3784 (1964).

Hagfors, T., and Morriello, J.E., "The Effect of Roughness on the Polarization of Thermal Emission from a Surface," J. Res. Natl. Bur. Standards 69D, 1614-1615 (1965).

Hagfors, T., Brockelman, R.A., Danforth, H.H., Hanson, L.B., and Hyde, G.M., "Tenuous Surface Layer on the Moon. Evidence Derived from Radar Observations," Science 150, 1153-1156 (1965).

Heiles, C. E., and Drake, F.D., "The Polarization and Intensity of Thermal Radiation from a Planetary Surface," Icarus 2, 281-292 (1963).

Hughes, V.A., "Radio Wave Scattering from the Lunar Surface," Proc. Phys. Soc. 78, 988-997 (1961).

Kac, M., "On the Distribution of Values of Trigonometric Sums with Linearly Independent Frequencies," Am. J. Math. LXV, 609-615 (1943).

Katz, I., "Wavelength Dependence of the Radar Reflectivity of the Earth and the Moon," J. Geophys. Res. 71, 361-366 (1966).

Keeping, K.J., "A Wide Band Antenna Having Axially Symmetrical Patterns, High-Gain and Low Side Lobes for All Polarizations," Report 46G-0008, Lincoln Laboratory, M.I.T. (1960), DDC 248360.

Klemperer, W.K., "Angular Scattering Law for the Moon at 6-meter Wavelength," J. Geophys. Res. 70, 3798-3800 (1965).

Krotikov, V.D., and Troitsky, V.S., "The Emissivity of the Moon at Centimeter Wavelengths," A.J. USSR 39, 1089-1093 (1962).

Long, M.W., "On the Polarization and Wavelength Dependence of Sea Echo," IEEE Trans. AP 13, 749-754 (1965).

Lynn, V.L., Sohigian, M.D., and Crocker, E.A., "Radar Observations of the Moon at 8.6-mm Wavelength," Technical Report 331, Lincoln Laboratory, M.I.T. (1963), DDC 426207. See also, J. Geophys. Res. 69, 781-783 (1964).

Mack, C.L., and Reiffen, B., "RF Characteristics of Thin Dipoles," Proc. IEEE 52, 533-542 (1964).

Metzger, P.G., "Polarization of Thermal Radiation of the Moon at 14.5 Gc/s," J. Res. Natl. Bur. Standards 69D, 1612 (1965).

Muhleman, D.O., "Radar Scattering from Venus and the Moon," Astron. J. 69, 34-41 (1964).

Peake, W.H., and Taylor, R.C., "Radar Backscattering Measurements from 'Moon-Like' Surfaces," Ohio State University E.E. Dept. Report 1388-9 (1963).

Prosser, R.T., "The Lincoln Calibration Sphere," Proc. IEEE 53, 1672 (1965).

Rea, D.G., Hetherington, N., and Mifflin, R., "The Analysis of Radar Echoes from the Moon," J. Geophys. Res. 69, 5217-5223 (1964).

Safran, H., "Backscattering Properties of Moon and Earth at X-Band," AIAA Journal 2, 100-101 (1964).

Salomonovich, A.E., and Losovsky, B.Y., "Radio Brightness Distribution of the Lunar Disk at 0.8 cm," Astron. J. USSR 39, 1074-1082 (1962).

Shaw, L., "Comments on 'Shadowing of Random Surfaces'," IEEE Trans. AP 14, 253 (1966).

Soboleva, N.S., "Measurement of the Polarization of Lunar Radio Emission on a Wavelength of 3.2 cm," Astron. J. USSR 39, 1124-1126 (1962).

Troitsky, V.S., "Theory of Lunar Radio Emission," Astron. J. USSR 31, 511-528 (1954).